Summary of AGN & SMBH

Jiacheng Peng

CONTENTS

1 Introduction of AGN

1.1 General properties

1. definition:
   objects emitting radiation that is fundamentally powered by accretion onto supermassive ($> 10^8 M_\odot$) black holes
   10% of galaxies are AGN.

2. Observational properties in general:

- Strong X-ray emission
- Relatively strong and non-thermal radio emission (extended structures in radio bands)
- Non-stellar emission from UV to IR
- Broad emission lines over a wide wavelength range (Not necessarily)
- Large variety of properties depending on the classification
- difference from stars:
  Accretion disk emission peaking in the UV band allows us to use **color index** to distinguish active galaxies from stars.

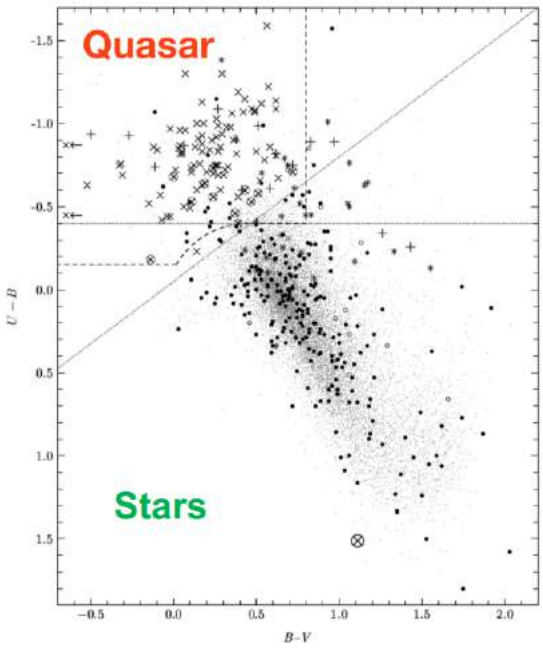

Figure 1: AGN color index

3. Energy output:
   gravitational energy production is the basis of the emission from AGN.

$$E \geq 10^{47}\text{erg/s} \times 10^{7}\text{yrs} \sim 3 \times 10^{61}\text{erg} \qquad (1)$$

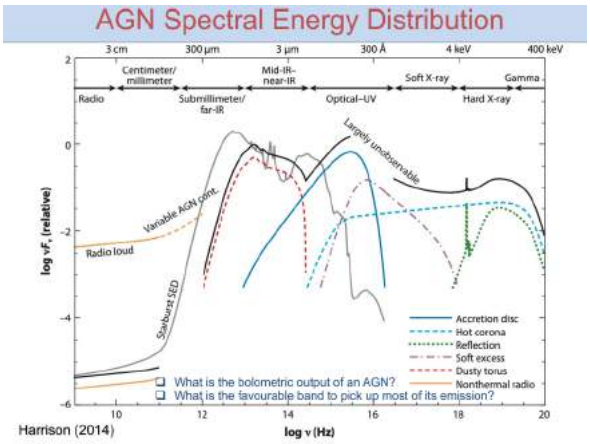

Figure 2: AGN SED

2 Accretion theory

2.1 Eddington Luminosity

The max luminosity allowed under the assumption of a spherically symmetric steady-state radial infall of ionized H
σ_T =Thomson cross-section

$$
\begin{aligned}
&P_{\rm rad} = \frac{F_{\rm rad}}{\rm c} = \frac{L}{4\pi R^2 c} \\
&F_{\rm rad} = \frac{L\sigma_T}{4\pi R^2 c} \\
&F_{\rm grav} = \frac{G\left(m_p + m_e\right)M}{\rm R^2} \approx \frac{G m_p M}{R^2} \\
&F_{\rm rad} \leq F_{\rm grav} \rightarrow \frac{L\sigma_T}{4\pi R^2 c} \leq \frac{GMm_p}{R^2} \rightarrow L \leq \frac{4\pi G c m_p}{\sigma_T} M \\
&\rightarrow L_{\rm Edd} = 1.26 \times 10^{38} \left(\frac{M}{M_{\rm sun}}\right) {\rm erg/s}
\end{aligned}
\tag{2}
$$

The Eddington accretion rate can be shown as:

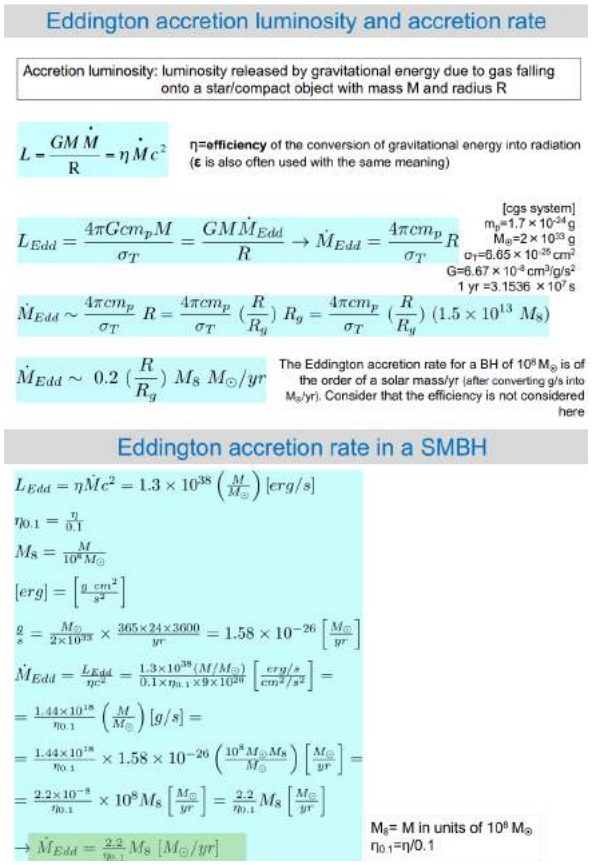

2.1.1 Eddington Time

1. when considering η.

$$
\begin{aligned}
t_{edd} &= \frac{M}{\dot{M_{edd}}} = \frac{M}{2.2 M_8/\eta_{0.1}} = 4.5 \times 10^7 \eta_{0.1} yr \\
t_{edd} &= \frac{M}{\dot{M_{edd}}} = \frac{L_{Edd}\sigma_T / 4\pi G c m_p}{L_{Edd}/(\eta c^2)} = \frac{\sigma_T \eta c}{4\pi G m_p}
\end{aligned}
\tag{3}
$$

without the efficiency term η:

$$
t_{edd} = \frac{\sigma_T c}{4\pi G m_p} \simeq 0.45 Gyr \tag{4}
$$

2. BH Growth: **What is not radiated is accreted.**
Salpeter time:

$$
\tau_{Salp} = \frac{\eta M_\bullet c^2}{L_{Edd}} = \frac{\eta M_\bullet c^2}{\frac{4\pi G c m_P M_\bullet}{\sigma_T}} = \frac{\eta \sigma_T c}{4\pi G m_P} \sim 4.5{\times}10^7 \eta_{0.1} {\rm yr} \tag{5}
$$

Accretion ⇒ 1. Energy production. 2. BH growth.
Eddington ratio:

$$
\begin{aligned}
&\lambda_{edd} = \frac{L_{acc}}{L_{Edd}} = \frac{L_{bol}}{L_{Edd}} \\
&Accretion: L_{acc} = \eta \dot{M_{acc}} c^2 \\
&Growth: \dot{M_b} h = (1-\eta)\dot{M_{acc}}
\end{aligned}
\tag{6}
$$

[PRO] BH growth obeys exponential law.
It's important to have BH seeds to form supermassive BHs.

$$
M_{BH}(t) = M_{BH_{\rm seed}} \ \exp\left((1-\eta)\lambda_{Edd}\frac{t}{\tau_{Salp}}\right) \tag{7}
$$

2.2 The accretion disc

2.2.1 Points of Viral Theorem

1. The central engine:
G.P.E ⇒ K.E. of infalling gas ⇒ **through viscosity**
Gas heating ⇒ Thermal emission

2. The role of Viral Theorem:
$E_{th} = 1/2\Delta E$ aka. Half of the released E goes into heat. (Dynamic analysis see the spectrum of disc part):

$$
\begin{aligned}
&2E_{kin} + E_{pot} = 0 \rightarrow E_{kin} = -\frac{1}{2}E_{pot} \\
&E_{kin} = E_{th,emi} = -1/2 E_{pot} \\
&dE_{kin} = -\frac{1}{2} dE_{pot} \\
&dE_{th} = -\frac{1}{2} GMdm\left(\frac{1}{r+dr} - \frac{1}{r}\right) = \frac{1}{2} GMdm\left(\frac{dr}{r(r+dr)}\right) \\
&dL = \frac{dE_{th}}{dt} = \frac{1}{2} GM\dot{M}\frac{dr}{r^2}
\end{aligned}
\tag{8}
$$

efficiency conversation factor from matter ⇒ Energy:

$$
\begin{aligned}
&L = \int_{R_{\rm out}}^{R_{\rm in}} dL = \frac{1}{2} GM\dot{M}\left[\frac{1}{r}\right]_{R_{\rm out}}^{R_{\rm in}} = \\
&\frac{1}{2} GM\dot{M}\left(\frac{1}{R_{\rm in}} - \frac{1}{R_{\rm out}}\right) \sim \frac{1}{2}\frac{GM\dot{M}}{R_{\rm in}} \\
&L = \eta \dot{M} c^2 \\
&\rightarrow \eta = \frac{GM}{2c^2 R_{in}}
\end{aligned}
\tag{9}
$$

e.g. ISCO: For Schwarzschild BH, $R_{ISCO} = 6GM/c^2$, $\eta \simeq 1/12 \sim 0.08$. It's difficult to understand the kinds of BHs.

3. Temperature-Mass/Radius relation:
In local equilibrium, assuming B.B. emission, from virial theorem we know $E_{heat} = 1/2\Delta E$ [PRO]:

$$\begin{aligned} L &= \frac{GM\dot{M}}{2r} = 2\pi r^2 \sigma T^4 \\ R_{in} &\approx R_S = 2GM/c^2 \\ R \gg R_{in} &\to 1 - (R_{in}/R)^{1/2} \approx 1 \\ R^{-3/4} &= (R/R_{\rm C})^{-3/4} \times \left(2GM/c^2\right)^{-3/4} \\ M_{\rm Edd} &= 2.2 M_8/\eta_{0.1} \quad [M_{\rm sun}/{\rm yr}] \end{aligned} \tag{10}$$

Then we can get:

$$T \propto M_8^{-1/4} \left(\dot{M}/\dot{M}_{\rm Edd}\right)^{1/4} ({\rm R}/{\rm R_S})^{-3/4} \ {\rm K} \tag{11}$$

$T(R) \propto R^{-3/4}$. $T(M) \propto M^{-1/4}$

4. Spin of BH

$$\begin{aligned} j = Jc/GM_{BH}^2 = a/M_{BH} \to \\ a = Jc/GM_{BH} = J/M_{BH} r_g c \\ R_{ISCO} = z\frac{GM}{c^2}, {\rm z} = {\rm r_{isco}}/r_{\rm g} \\ \eta = 1 - \left[1 - \frac{2}{3z}\right]^{1/2} \end{aligned} \tag{12}$$

high η means less mass available for SMBH growth.

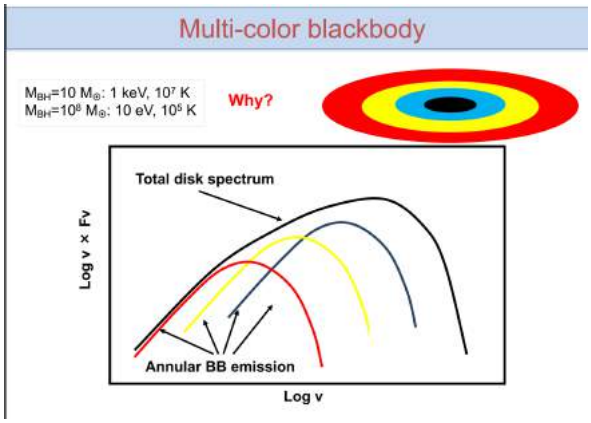

Figure 3: AGN disk spectrum: combination of multiple BB components

2.2.2 Points of Viscosity

The role of viscosity:

- For the accretion disk, it should allow the accreting material to go down to the next stale orbit and in the end accreted by the SMBH.
- However, angular momentum in pure Bondi accretion is in absence. We need angular momentum conservation in the SMBH system.
- The gas in the accretion disk loses angular momentum through viscosity and produce thermal emission.

FOR GEOMETRICALLY THIN DISCS

Assumption: $M_{disc} \leq\leq M_{BH}$. $H \leq\leq r$(optically thin)

1. Keplerian rotation: Instead of solid rotation, Keplerian rotation allows the angular momentum transfering from annulus to annulus because of shear force.
the annuli closer to the compact object move faster than the outer ones:

$$v_\phi\,(r - \lambda/2) = \Omega(r - \lambda/2) \times (r - \lambda/2) > v_\phi(r + \lambda/2) \tag{13}$$

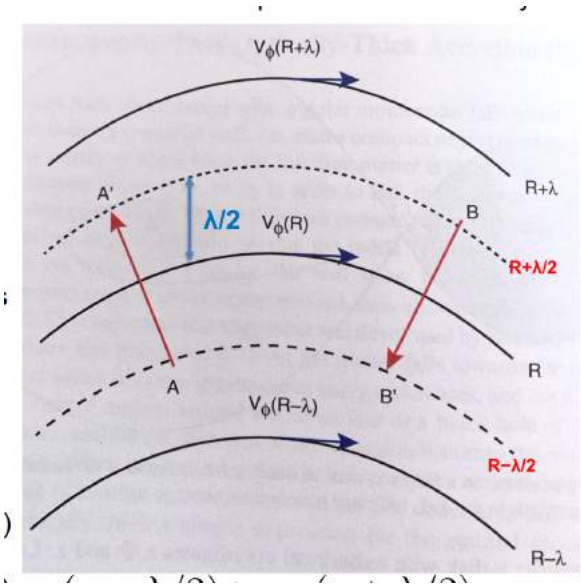

Figure 4: Keplarian Orbits

2. viscosity$\nu = \lambda\bar{v}$.

- Kinematic viscosity: λ: mean free path. v: thermal speed of the molecules. case of molecular transport in shearing motion
- Turbulence viscosity: λ: spatial scale or characteristic wavelength of the turbulence. v: tpyical velocity of the eddies.

$$\nu = \alpha c_S H \tag{14}$$

3. Momentum changing = Torque changing:

$$\begin{aligned} &= \dot{M}_A \times (r + \lambda/2) \times \Omega(r - \lambda/2) \times (r - \lambda/2) - \dot{M}_B \\ &\times (r - \lambda/2) \times \Omega(r + \lambda/2) \times (r + \lambda/2) = \\ &= \dot{M}_A \times \left(r^2 - \lambda^2/4\right) \times \Omega(r - \lambda/2) - \dot{M}_B \\ &\times \left(r^2 - \lambda^2/4\right) \times \Omega(r + \lambda/2) \sim \\ &\sim \dot{M}_A \times r^2 \times \Omega(r - \lambda/2) - \dot{M}_B \times r^2 \times \Omega(r + \lambda/2) \\ &Surface\ mass\ density\ of\ the\ disc : \Sigma = \rho H \\ &\dot{M}_A = \dot{M}_B = (2\pi r H)\rho(r)\bar{v} = 2\pi r \Sigma \bar{v} \end{aligned} \tag{15}$$

- For Keplarian orbits, $d\Omega/dr \leq 0$, so G(r) $\leq$ 0, inner rings lose J to outer ones and gas spirals in.

$$G(r) = 2\pi r\Sigma\nu r^2\frac{d\Omega}{dr} = 2\pi r\Sigma\nu r^2\Omega \tag{16}$$

- net torque:

$$\begin{aligned} G(R+dR) - G(R) &= \frac{\partial G}{\partial R}dR \\ \Omega\frac{\partial G}{\partial R}dR &= \left[\frac{\partial(G\Omega)}{\partial R} - G\Omega'\right]dR \end{aligned} \tag{17}$$

$\frac{\partial(G\Omega)}{\partial R}dR$: Convection rate throught gas by torques; Integrated from inner edge to the outer edge we get the all rotational energy tranferred through torque process
$-G\Omega' dR$: loss rate of mechanical energy transferred into internal energy which is dissipated by the disc and irradiated by the disc as B.B. or Multi-B.B.

- viscous dissipation:
The viscous torques cause viscous dissipation within the gas at the rate reported above per ring of width dR
This energy will be irradiated by the upper and lower faces of the disc.
rate of viscous dissipation per unit plane surface area.

$$D(R) = \frac{9}{8}\nu\Sigma\frac{GM}{R^3} \tag{18}$$

prove:

$$\begin{aligned} D(R) &= \frac{G\Omega' dR}{4\pi RdR} = \frac{G\Omega'}{4\pi R} = \frac{\left(2\pi R\Sigma\nu R^2\Omega'\right)\Omega'}{4\pi R} \\ &= \frac{1}{2}\Sigma\nu\left(R\Omega'\right)^2 (1) \end{aligned} \tag{19}$$

Using Keplerian obits into :

$$\Omega = \left(\frac{GM}{R^3}\right)^{1/2} (2) \tag{20}$$

Take (2) into (1) then we get the result.

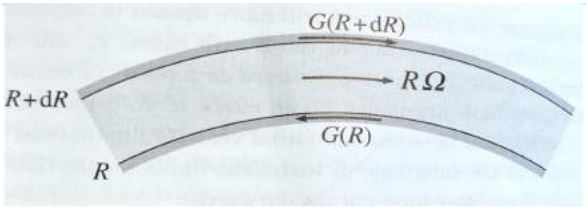

Figure 5: GR

4. Reynolds number:
Measures the importance of viscosity.

$$R_e = \frac{\text{inertia}}{\text{viscous}} \sim \frac{v_\phi^2/R}{\lambda\bar{v}v_\phi/R^2} = \frac{Rv_\phi}{\lambda\bar{v})} \tag{21}$$

$R_e \leq\leq 1$: Molecular Viscous force dominances the flow.
$R_e \geq\geq 1$: Turbulence viscosity dominances.

5. conservation laws in radial disc structure :
Net flow from neighbouring annuli (R and $R+\Delta R$) should obey mass and momentum conservation law.

- Mass:

$$\begin{aligned} &M = 2\pi R\Delta R\Sigma \\ &\frac{\partial}{\partial t}(2\pi R\Delta R\Sigma) =\sim -2\pi\Delta R\frac{\partial}{\partial R}\left(R\Sigma v_R\right) \\ &\Delta R \to 0 \Rightarrow R\frac{\partial\Sigma}{\partial t} + \frac{\partial}{\partial R}\left(R\Sigma v_R\right) = 0 \end{aligned} \tag{22}$$

- Momentum:

$$\begin{aligned} &P = 2\pi R\Delta R\Sigma R^2\Omega \\ &G(R+dR) - G(R) = \frac{\partial G}{\partial R}dR \\ &\Delta R \to 0 \Rightarrow R\frac{\partial}{\partial t}\left(\Sigma R^2\Omega\right) + \frac{\partial}{\partial R}\left(R\Sigma v_R R^2\Omega\right) = \frac{1}{2\pi}\frac{\partial G}{\partial R} \\ &R\Sigma v_R\left(R^2\Omega\right)' = \frac{1}{2\pi}\frac{\partial G}{\partial R} \end{aligned} \tag{23}$$

For steady-state accretion and so a stable thin disc, $\frac{\partial}{\partial t} = 0$in conservation laws.

6. timescales

$$t_{visc} = \frac{R^2}{\nu} = \frac{R^2}{\alpha c_S H} = \frac{R^2}{\alpha v_K H^2/R} = \frac{R}{\alpha v_K}\left(\frac{R}{H}\right)^2 = \frac{1}{\alpha\Omega}\left(\frac{R}{H}\right)^2$$

$$t_{visc} \sim 260\,\frac{M}{10^8 M_\odot}\frac{0.1}{\alpha}\left(\frac{H}{0.01R}\right)^2\left(\frac{R}{30R_G}\right)^{3/2}[yr]$$

Viscous (radial drift/inflow) timescale

$$t_{dyn} = \frac{1}{\Omega} \sim 1\,\frac{M}{10^8 M_\odot}\left(\frac{R}{30R_G}\right)^{3/2}[day]$$

Dynamical timescale

$$t_{th} = \frac{\Sigma c_S^2}{D(R)} \sim \frac{\Sigma c_S^2}{\Sigma\nu GM/R^3} = \frac{c_S^2}{\alpha c_S H\Omega^2} = \frac{c_S}{\alpha H\Omega^2} = \frac{v_K H/R}{\alpha H\Omega^2} = \frac{(R\Omega)H/R}{\alpha H\Omega^2} = \frac{1}{\alpha\Omega}$$

$$t_{th} \sim 9\,\frac{M}{10^8 M_\odot}\frac{0.1}{\alpha}\left(\frac{R}{30R_G}\right)^{3/2}[day]$$

Thermal timescale

Figure 6: timescales

7. The Luminosity and the spectrum function of disc:
For steady thin disc:

$$\begin{aligned} &\nu\Sigma = \frac{\dot{M}}{3\pi}\left[1 - \left(\frac{R_\star}{R}\right)^{1/2}\right](1) \\ &D(R) = \frac{9}{8}\nu\Sigma\frac{GM}{R^3}(2) \\ &L\left(R_1, R_2\right) = 2\int_{R_1}^{R_2} D(R)2\pi RdR \\ &= \frac{3GM\dot{M}}{2}\int_{R_1}^{R_2}\left[1 - \left(\frac{R_\star}{R}\right)^{1/2}\right]\frac{1}{R^2}dR \\ &\text{if } R_1 = R_\star, R_2 \to \infty \Rightarrow L_{disc} = \frac{3GM\dot{M}}{2}\left\{\frac{1}{R_\star}\frac{1}{3} - 0\right\} \\ &L_{disc} = \frac{GM\dot{M}}{2R_\star} = \frac{1}{2}L_{acc} \end{aligned} \tag{24}$$

At any radius:the energy dissipation rate
= **release of gravitational binding energy** $\frac{GM\dot{M}dR}{2R^2}$
+ **energy loss due to angular momentum transport (outwards)** $\frac{GM\dot{M}}{R^2}\left[1-\frac{3}{2}\left(\frac{R_\star}{R}\right)^{1/2}\right]dR$

General form of Luminosity (energy dissipation rate):

$$LdR = -\left(\frac{dE}{dt}\right)dR = \frac{3GM\dot{M}}{2R^2}\left[1-\beta\left(\frac{R_{in}}{R}\right)^{1/2}\right]dR \tag{25}$$

$$L = \left(\frac{3}{2}-\beta\right)\frac{GM\dot{M}}{R_{in}} \tag{26}$$

$\beta \leq 1$ depends on the magnetic content of accretion flow within ISCO.

$$\sigma T^4(R) = D(R) = \frac{3GM\dot{M}}{8\pi R^3}\left[1-\left(\frac{R_\star}{R}\right)^{1/2}\right]$$
$$\rightarrow T(R) = \left\{\frac{3GM\dot{M}}{8\pi R^3\sigma}\left[1-\left(\frac{R_\star}{R}\right)^{1/2}\right]\right\}^{1/4}$$
$$R >> R_\star \rightarrow T = \left(\frac{3GM\dot{M}}{8\pi R_\star^3\sigma}\right)^{1/4}\left(\frac{R}{R_\star}\right)^{-3/4} \propto R^{-3/4}$$
$$F_\nu = \frac{2\pi\cos i}{D^2}\int_{R_\star}^{R_{\rm out}} I_\nu R dR$$
$$= \frac{4\pi h\cos i\nu^3}{c^2D^2}\int_{R_\star}^{R_{\rm out}}\frac{RdR}{e^{h\nu/kT(R)}-1} \tag{27}$$

If we use x:

$$x = \frac{h\nu}{kT(R)} \sim \frac{h\nu}{kT_\star}\left(\frac{R}{R_\star}\right)^{3/4}$$
$$\rightarrow F_\nu \propto \nu^{1/3}\int_0^\infty \frac{x^{5/3}}{e^x-1}dx \propto \nu^{1/3} \tag{28}$$

Then we obtain the B.B. component in AGN spectrum

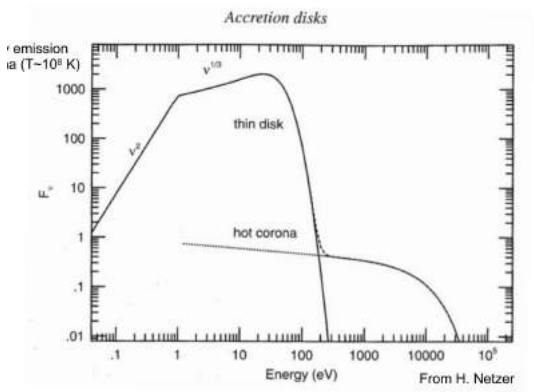

Figure 7: B.B.+Hot cornoa

8. Hydrodynamics equilibrium:
At a given radius both pressure and temperature are vertical and decoupled.

$$\frac{1}{\rho}\frac{\partial P}{\partial z} = -\frac{GMz}{R^3}$$
$$\rho(R,z) = \rho_c(R)e^{-z^2/2H^2}$$
$$assume\ : T(R,z) \sim T_C(R) = T(R,0)$$
$$P = \frac{k\rho T_C}{\mu m_P} + \frac{4\sigma}{3c}T_C^4 \tag{29}$$
$$F(z) \sim (4\sigma/3\tau)T^4(z)$$
$$\text{If } T_C^4 >> T^4(H) \rightarrow (4\sigma/3\tau)T_C^4 = D(R)$$

FOR INEFFICIENT ACCRETION FLOWS

1. ADAF solution:
Lower accretion rate
→ lower surface density than geometrically thin discs: optically thin, geometrically thick
→ cooling rate $\propto {N_e}^2$, inefficient cooling in discs, higher temperatures of particles (viral temperature)
→ E_{grav} deposited in disc by viscosity retains in the accretion flow as the internal energy of ions but not efficiently transferred to radiation
→ low lunimosity
→ Two-temperature disc if the accretion disc is extended as a standard efficient accreted disc

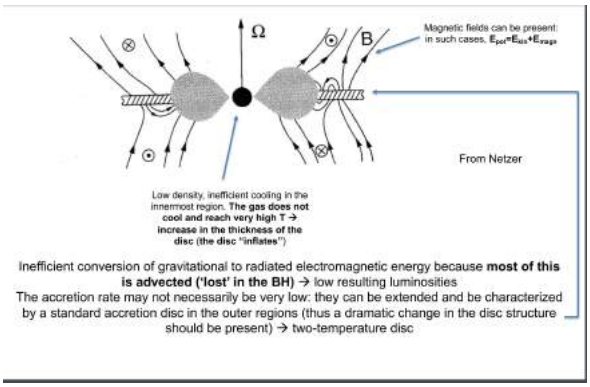

Figure 8: ADAF

2. Calculations of Temperature:

particles are heated close to viral temperature

$$\frac{1}{2}mv^2 = 3kT$$
$$mv^2 = \frac{GMm}{R}$$
$$r = R/R_S = \frac{R}{2GM/c^2}$$
$$T = \frac{GMm}{6krR_S} = \frac{GMm}{6kr2GM/c^2} = \frac{mc^2}{12kr} \quad (30)$$
$$T_i = \frac{m_p c^2}{12kr} \sim \frac{10^{12}}{r}K$$
$$T_e = \frac{m_e c^2}{12kr} \sim \frac{10^9}{r}K$$
$$T_i T_e \Rightarrow inefficient\ cooling$$

3. Calculations of energy conservation:
n/dsic element/unit time: $nvd\sigma$
n: surface number density; v: radial velocity v(r); sigma: surface element. nv: radial flux.

$$\frac{du_{adv}}{dr} = T\frac{ds}{dr} \rightarrow \frac{dU_{adv}}{dt} = nvT\frac{ds}{dr} = Q^+ - Q^- \quad (31)$$

$Q+$: E_{grav} transferred to the plasma by viscous processes = (D(R))
$Q-$: Energy radiated by the plasma by all processes
In geometrically thin discs, Q+=Q-. In ADAF discs, $Q+ \gg Q-$: an element of the gas is unable to radiate its thermal energy in less time than it takes to be transported through the disc onto the BH. So cooling $\ll$ heating. L(ADAF) $\ll$ L(SS73).

4. Evolution of accretion modes
$\dot{M}_{cri} \sim 0.4\alpha^2 \dot{M}_{edd}$??

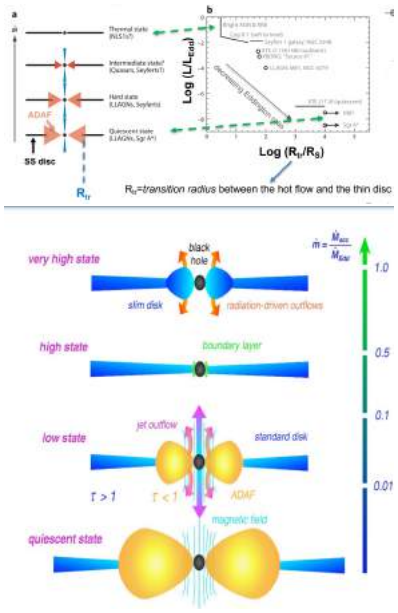

Figure 9: ADAF evolution

3 Emission Mechanisms

3.1 Continuum

3.1.1 Thermal

Cooling time:

$$t_{cool} = \frac{E}{|dE/dt|} = \frac{3/2\,(n_e + n_i)\,kT}{j_v(T)} \tag{32}$$

1. Bremmstrahlung(FREE-FREE):

- Free-free columb collisions
- Intensity distribution:
  $hv << kT$, opt.thick:

$$I_v = B_v \propto v^2 \tag{33}$$

  $hv << kT$,opt.thin:

$$I_v = B_v\tau_v \propto v^2\tau_v \propto v^2\left(v^{-2}T^{-3/2}\right) = \text{ cons} \tag{34}$$

  $hv >> kT$, opt.thin:

$$I_v \approx B_v(T)\tau_v \approx \left(v^3 e^{-hv/kT}\right)\left(v^{-3}T^{-1/2}\right) \propto e^{-hv/kT} \tag{35}$$

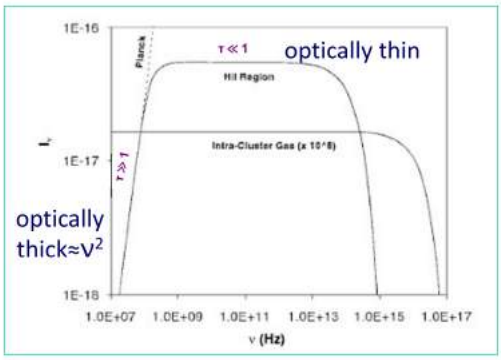

Figure 10: Bremms

- Cooling time:

$$t_{cool} \approx \frac{6\times 10^3}{n_e Z^2 \bar{g}_{ff}} T^{\frac{1}{2}} yr \tag{36}$$

  e.g.:
  Clusters of galaxies: a few times of 10^{10}years.$n_e \simeq 10^3 cm^{-3}, T \simeq 10^8 K$
  HII region: 1000 yrs. $n_e \simeq 100 - 1000 cm^{-3}, T \simeq 1000 - 10000 K$

- Polarization:
  Polarized with the electric vector perpendicular to the palne of interaction. In most astrophysical cases, the planes of interactions are randomly distributed resulting in null net polarization.
  Anisotropic distribution of electron–polarized.

2. Blackbody:
   The optically thick situation of Bremms.

- Plank function:

$$I(v,T) = \frac{2hv^3}{c^2}\frac{1}{e^{hv/kT}-1} \tag{37}$$

- Stefan-Boltzmann Law:
  u(T):spectral energy density integrated in frequency $[J/m^3]$

$$\begin{aligned} u(T) = \int_0^\omega \mu(\nu,T)d\nu &= \tfrac{4\pi}{c}\int_0^\omega I(\nu,T)d\nu \\ &= \tfrac{4}{c}\sigma_{SB}T^4 = aT^4 \\ a &= \tfrac{4\sigma_{SB}}{c} \end{aligned} \tag{38}$$

- Approximations and Wien Law:
  $hv << kT$ R-J Approximation [PRO] with Taylor Expasion

$$I(v,T) = \frac{2v^2}{c^2}kT \propto v^2 T \tag{39}$$

  $hv >> kT$ Wien Approximation:

$$I(v,T) = \frac{2hv^3}{c^2}e^{-hv/kT} \tag{40}$$

  Wien Law:

$$\begin{aligned} hv_{\text{peak}} &= 2.82\text{kT} \\ v_{\text{peak}}\,(\text{Hz}) &= 5.88\times 10^{10}\ \text{T(\ K)} \end{aligned}$$

  CMB peak = 1.06 mm

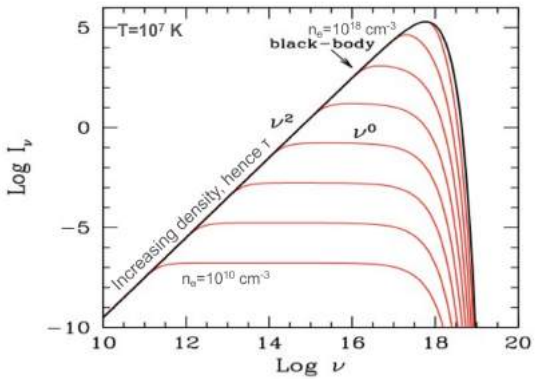

Figure 11: Bremms-Blackbody

3.1.2 Non-thermal

1. Synchroton

- Mechanism:
  Relativistic e^- spiraling around magnetic field ⇒ electron acceleration ⇒ K.E. losing via radiation of photons.
- Intensity Function:

$$I(v) \propto N_0 B^{(\delta+1)/2} v^{-\alpha} = N_0 B^{\alpha+1} v^{-\alpha} \propto v^{-\alpha} \tag{41}$$

  power-law.

- Cooling time:

$$t_{cool} \approx \frac{7.75 \times 10^8}{B^2 \gamma} s \quad t_{cool} \propto B^{-2} \tag{42}$$

e.g.
ISM:$B \simeq$ a fewμG, $\gamma \simeq 10^4$, $t \simeq 10^8 yr$.
Radio Galaxy: $B \simeq 10^3 G$, $\gamma \simeq 10^4$, $t \simeq 0.1 s$. Continuous acceleration??

- Polarization:
The radiation is linearly polarized perpendicularly to the projection of B on the plane of the sky.
Upper limit:
opt.thin: $\Pi = \mathrm{P/I} = (3\delta + 3)/(3\delta + 7)$
opt.thick: $\Pi = \mathrm{P/I} = 3/(16\delta + 13)$

2. Compton Scattering:

- energy: ph $\Rightarrow e^-$

- wavelength shift:

$$\lambda - \lambda_0 = \frac{h}{m_e c}(1 - cos\theta) \tag{43}$$

3. Inverse Compton Scattering:

- energy: e $\Rightarrow$ ph

- emissitivity:

$$j_{IC}(\boldsymbol{v}) \propto \boldsymbol{v}^{-(\delta-1)/2} = \boldsymbol{v}^{-\alpha} \tag{44}$$

- IC Cooling time:
Energy loss per electron of Synchroton and IC:

$$\begin{aligned} &-\left(\frac{dE}{dt}\right)_{IC} \approx \frac{4}{3}\sigma_T c \gamma^2 \beta^2 \; U_{ph} \; U_{ph} = n_{ph} h v_{av} \\ &-(dE/dt)_{Sync} = \frac{4}{3}\sigma_T c \beta^2 \gamma^2 U_B \; U_B = B^2/8\pi \\ &\textit{magnetic energy density}\,(u_m) \end{aligned} \tag{45}$$

4. Comptonization:

- Comptonization parameter:

$$y = \frac{kT_\mathrm{e}}{m_\mathrm{e} c^2} \max\left(\tau_\mathrm{e}, \tau_\mathrm{e}^2\right) \tag{46}$$

Conditions for significant distortion of the photon spectrum by Comptonization: $4y \leq 1$

- Spectrum Shape:
Kompaneets equation:

$$\frac{\partial n}{\partial y} = \frac{1}{x^2}\frac{\partial}{\partial x}\left[x^4\left(n + n^2 + \frac{\partial n}{\partial x}\right)\right] \quad \begin{aligned} &\mathrm{n} = \text{ occupational number} \\ &x = \hbar\omega/kT_\mathrm{e} \end{aligned} \tag{47}$$

Low f: power-law $I(\omega) \propto \omega^{3+m}$

$$\begin{aligned} m &= -\frac{3}{2} - \left(\frac{9}{4} + \gamma\right)^{1/2} \\ \gamma &= \frac{\pi^2}{3}\frac{m_\mathrm{e} c^2}{\left(\tau + \frac{2}{3}\right)^2 kT_\mathrm{e}} \quad \text{(spherical)} \\ \gamma &= \frac{\pi^2}{12}\frac{m_\mathrm{e} c^2}{\left(\tau + \frac{2}{3}\right)^2 kT_\mathrm{e}} \quad \text{((disc)} \end{aligned} \tag{48}$$

High f: exponential/Wien, cut-off depends on kT_e of e.

$$I(\omega)\mathrm{d}\omega = \frac{\hbar\omega^3}{\pi^2 c^2} n(\omega)\mathrm{d}\omega = \frac{\hbar\omega^3 \mathrm{e}^{-\hbar\omega/kT_\mathrm{e}}}{\pi^2 c^2}\,\mathrm{d}\omega \tag{49}$$

- Astrophysical examples:

1) Synchrotron Self-Compton:
Relevant in blazars.

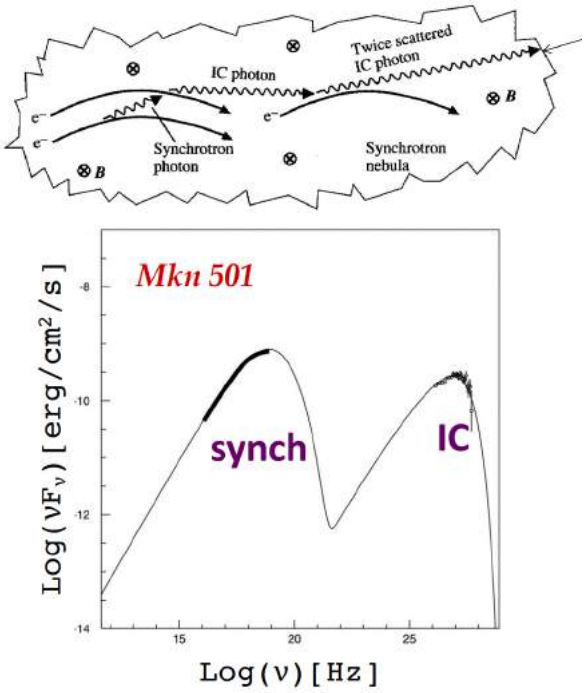

Figure 12: SSC

2) Polarization in blazars:
Degree of polarization depends on the geometry of the system.
Radiation field in blazars: SSC or external IC (thermal emission from the accretion disc). In SSC, same pol.angle for IC and Synch.

3) Sunyaev-Zeldovich effect:
IC between CMB low-E photons and energetic e in the plasma/cluster of gals.
$y \sim 10^{-3} - 10^{-4}$
Used to estimate the baryonic mass fraction and Hubble constant.

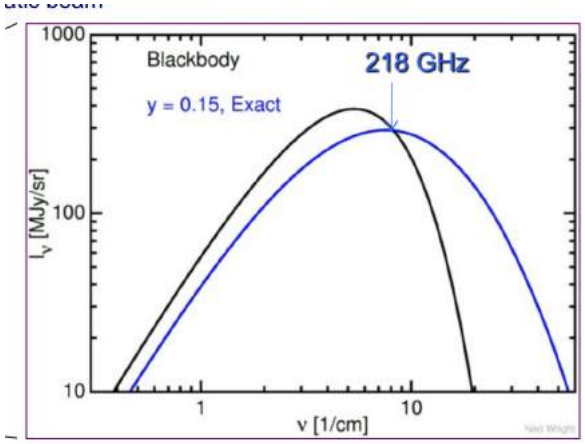

Figure 13: S-Z effect

3.1.3 Chrenkov Radiation

- Mechanism: pair production+bremms.
  γ-ray⇒pair production of porsitrons and electrons ⇒ Bremss.+pair production. ⇒ electromagnetic cascade.

- Final detectable product: Chrenkov light (faint short-lasting (3-5 ns) beam of blue light)

- Maximum number of particles: $N_{max} = E_0/E_C, E_C = 84Mev$ lower limit. Below it the ionizaiton loss dominates.

- Shower angle: $\theta = cos^{-1}(1/(n\beta)), \beta = v/c$

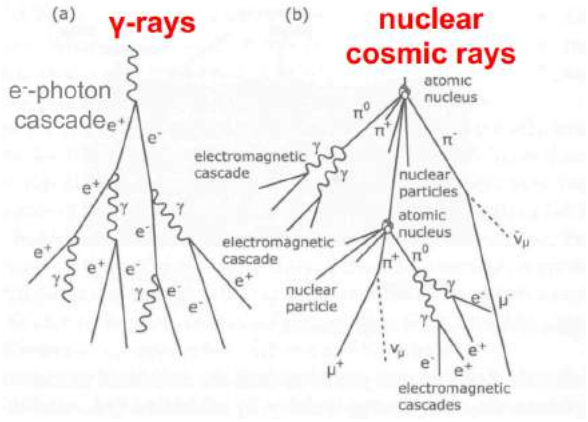

Figure 14: Chrenkov

3.2 Emission Lines

3.2.1 Einstein's coefficients

- $J = J_v = \frac{1}{4\pi}\int I_v dv$ intensity of the radiation field [PRO]At equilibrium, $J_v = I_{v,Blackbody}$:

$$
\begin{aligned}
n_1 B_{12} J_v &= n_2 A_{21} + n_2 B_{21} J_v \\
J_v &= \frac{A_{21}/B_{21}}{(n_1/n_2)\,(B_{12}/B_{21}) - 1} \\
\frac{n_1}{n_2} &= \frac{g_1}{g_2}\frac{e^{-E/kT}}{e^{-(E+hv)/kT}} = \frac{g_1}{g_2} e^{hv_{21}/kT}
\end{aligned}
\tag{50}
$$

- Simulated emission:
  The energy of the emitted photon is simulated by the presence of radiation field.
  Coherent emission: Same E, Same direction, Same phase.(e.g.laser, maser)

3.2.2 Bound-Bound

1. Photon excitation and de-excitation

- EW:

$$EW = \int \frac{F_C - F_v}{F_C} dv \tag{51}$$

- Estimation of ion numbers and transition strength $EW = f(N_H)$:

$$
\begin{aligned}
&\frac{F_v}{F_C} = e^{-\tau_v} \rightarrow \\
&EW = \frac{\lambda^2}{c}\int \left(1 - e^{-\tau_v}\right) dv \overset{\tau_{\tau<1(ISM)}}{\longrightarrow} \frac{\lambda^2}{c}\int \tau_v dv \\
&\tau_v = \left(\frac{\pi e^2}{m_e c^2}\right) \mathrm{N_i f_v} \phi(v) \\
&\mathrm{EW} = \left(\frac{\pi e^2}{m_e c^2}\right) \mathrm{N_i f_\lambda} \lambda^2
\end{aligned}
\tag{52}
$$

  N_i =number of absorbers.
  f = oscillator strength
  $\phi(v)$ = line profile

- Curve of Growth:
  Optical depth ↑, line saturates, Doppler core ⇒ lorentzian wings

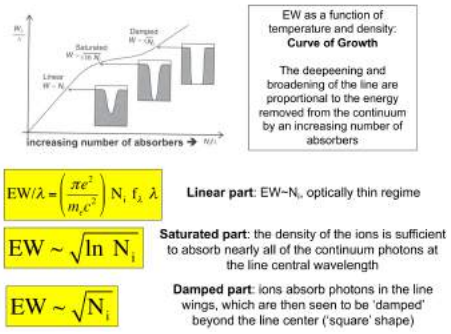

Figure 15: curve of growth

2. Coliisional excitation/de-excitation
   No radiation.

3.2.3 Bound-Free

1. ionization/recombination See Fig.15 for recap of 3 ionizaiton methods and 3 recombination methods.

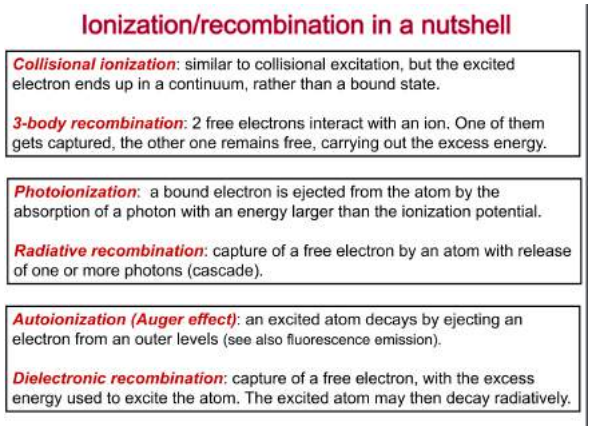

Figure 16: recap

- photoelectric absorption:
  $\sigma_{ph} \propto E^{-3.5}$

2. Flourecence lines and Auger Effect

- Mechanism:
  ionization occurs in an inner shell, the atom is in both excited and ionized. De-excitation can be:

1) Fluorescence emission: e in outer shell fills the vacancy and emits a photon.
   $L \to K : K\alpha, M \to K : K\beta$.
   Fluorescence yield: the probability that the shell is fill of a radiative transition but not auger effect

$$Y_Z^K \approx \frac{N_K}{n_{vK}} \qquad I_{K-line} = Z(abundance) \times Y \tag{53}$$

   N_K: Number of K-shell X-ray photons emitted
   n_{vK}: Number of primary vacancies.
   [PRO]Why we mainly observe Fe line?

2) Auger effect: Double-ionization but not radiation. After the filling of the outer e, the released energy kicks out another outer e. electron, which is called Auger electron.

3. Dielectronic recombination: Astrophysical application: Determining the elemental abundances of cosmic gas clouds

3.2.4 Line profiles

1. Natural Broadening

- Mechanism: Uncertainty principle.

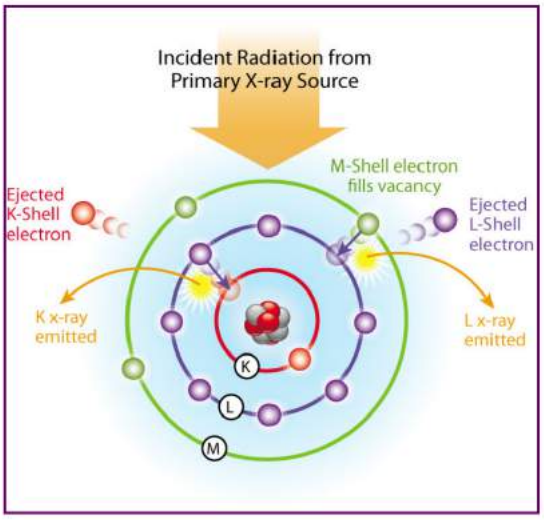

Figure 17: Flourescence emission

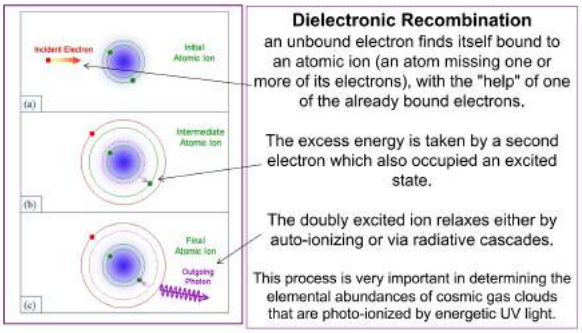

Figure 18: dielectronic

- Shape: Lorentzian shape, dumping profile-line wing.

$$\phi(v) = \frac{\gamma/4\pi^2}{(v - v_0)^2 + (\gamma/4\pi^2)} \tag{54}$$

2. Thermal Broadening

- Mechanism: Atoms in the gas follow MB velocity distribution.

- Shape: Gaussian component-line core.
  Natural+thermal:

$$\phi(v) = \frac{1}{\sigma\sqrt{\pi}} e^{-\frac{(v-v_0)^2}{\sigma^2}} \qquad \sigma = \frac{v_0}{c}\sqrt{\frac{2kT}{m}} + \zeta(microturbolence) \tag{55}$$

3.2.5 equilibrium

1. Collisional equilibrium: collisional ionization rate = recombination rate

- Line cooling by line emission:
  The main continuum emission process in a plasma is thermal bremsstrahlung: $j_{br} \propto T^{1/2} n_i n_e$

$$t_{\text{cool, br}} \propto (n_e + n_i)\, kT/j(T) \approx T^{1/2} (dominace > 2keV)$$
$$t_{\text{cool, lines}} \propto T/T^{-0.7} \approx T^{1.7} (dominace < 2keV) \tag{56}$$

2. Photoionization equilibrium: photoionization rate = recombination rate

- Ionization parameter U/Ξ: determine the ionization structure
  ionizing photon flux/electron density

$$U = \frac{\int_{v_0}^{\infty} \frac{F_v}{hv} dv}{n_e} \text{ or } \Xi \propto \frac{U}{T} \propto \frac{\text{rad. pressure}}{\text{gas pressure}} \tag{57}$$

- Compton Temperature:

$$T_C = \frac{h < \nu >}{4k} \tag{58}$$

  photoionization equilibrium ⇒ T doesn't change ⇒ matter completely ionized ⇒ Compton Scattering dominance.

3. [PRO]AGN emission processes applications.

4 Unification Model and Classification

4.1 Strict and Weak Unification

1. Strict Unification:

1) Orientation

2) Obscuring materials (dust torus).

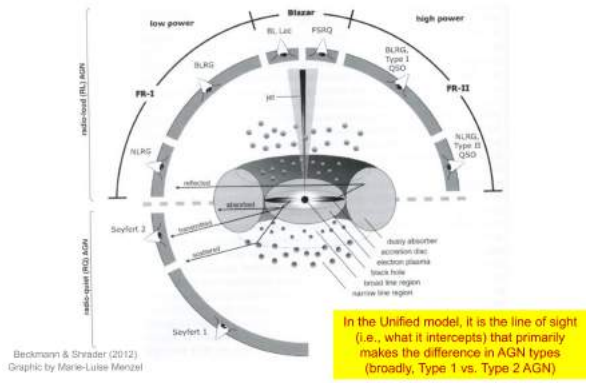

Figure 19: Strict Unification

2. Weak Unification:

1) Black hole accretion rate (L/L_{Edd}):
change the structure and emission properties of the accretion flow and thus the SED shape and excitation properties of surrounding gas

2) Jet strength:
strength of a relativistic jet can vary, yielding very different multi-wavelength signatures particularly in the radio and γ-rays

3) Covering factor of dust torus:
producing a statistical difference in the intrinsic properties of objects that are observed to be type 2 as opposed to type 1

4) Orientation

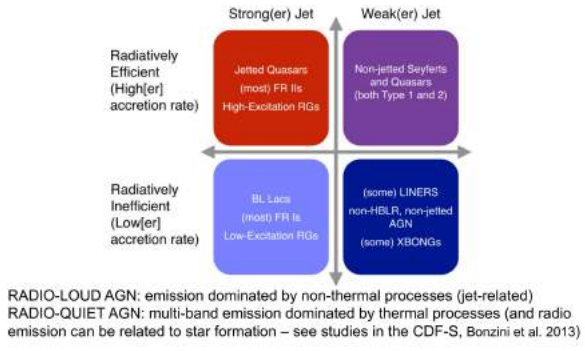

Figure 20: weak unification: jet and accretion rate

4.2 Classification Criteria

4.2.1 Seyfert Galaxies

1. Type 1 AGN: (Unobscured)

- Emission: Broad opt./UV permitted emission lines (FWHM$\sim 1500-15000 km/s$) + Narrow forbidden lines(FWHM$\sim 500-1000 km/s$)
Collisional de-excitation dominates over forbidden line emission

- Number density: $n \sim 10^{9-10} cm^{-3}$

2. Type 2 AGN: (Obscured)

- Emission: Narrow permitted lines + Narrow forbidden lines
FWHM of forbidden lines: $Starburst < Type2AGN < permitted$

- Number density: $n \sim 10^{3-5} cm^{-3}$

3. X-ray division:

- $N_H < 10^{22} cm^{-2}$ (column density): Type1/1.2. lower absorption in spectrum

- $N_H > 10^{22} cm^{-2}$: Type 1.8/1.9/2. The most strongly absorbed sources.

4. How to define the intermediate type of seyfert galaxies?
Arbitrary defination: relative width of H_β. $FWHM_{H_\alpha}/FWHM_{H_\beta}$

4.2.2 Quasars

1. Quasar and Seyfert:

- Quasars: Higher luminosity than seyfert galxaies.

- Seyfert galaxies with $M_B < 23 mag$: Quasars.

2. Type 1 and Type 2: Same as Seyfert.

3. Emission: Big blue bump at $\lambda = 100-400 nm$

- [PRO]Why the big blue bump is not from the starlight of the host galaxy?

4. Radio-loud and Radio-quiet:

- Radio hardness: $R = log\frac{f_{radio}}{f_B}$, $R < 1$,Radio quiet, $R > 1$, Radio loud.
radio: luminosity at 1-6GHz. Opt.: luminosity at B band.

4.2.3 Radio Galaxies

Classification based on morphology and radio power.

1. Morphological classification: FR I/FR II
Division: $L_R = 10^{32} ergs^{-1} Hz^{-1} sr^{-1}$ at 175MHz

- FR I: Low L, 2-sided jets,edge-darkened radio lobes, inefficient engine, radio-mode feedback;

- FR II: High L, (some cases)1-sided jet, edge-brightened radio lobes dominated, efficient engine, quasar-mode feedback
- Flat and steep:

$$S_\nu \propto \nu^{-\alpha} \tag{59}$$

$\alpha \geq 0.5$: Steep spectrum, extended sources
$\alpha \leq 0.5$: Flat spectrum, compact sources

2. Radio power classification: Radio-loud/Radio-quiet
- Radio over Opt. : $R_L = \frac{F(5GHz)}{F(4400\dot{A}} > 10$
- Radio over X-ray : $logR_X = \frac{vL_v(5GHz}{L_X} > -4.5$
- Around 10% of AGN are RL.

3. Radio power classification: Low/High-excitation RGs
- LERG: Low accretion efficiency($L_{edd}/L < 0.1$), ADAF accretion, fuelled by hot gas IGM, highly efficient in collimated jet production.
- HERG: High accretion efficiency($0.1 < L_{Edd}/L < 1$), classic disk, fuelled by cold gas IGM, (on average) less likely to launch jet
- Optical classification of L/HERG:

$$EI = \log([OIII]/H\beta) - \frac{1}{3}[\log([NII]/H\alpha) + \log([SII]/H\alpha) + \log([OI]/H\alpha)] \tag{60}$$

$EI > 0.95$, RL. $EI < 0.95$, RQ.

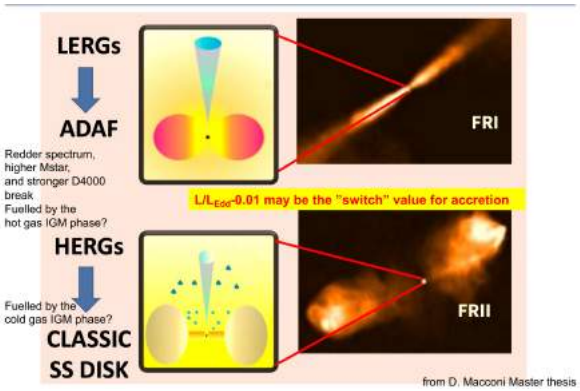

Figure 21: LERG HERG

4.2.4 Blazars

General properties:

- Featureless, Strong and fast variability (due to the orientation as following). Prominent emitters from radio to VHE(1 Tev) and dominance by non-thermal continuum.
- Pointing at the observer, or very close to the observer's l-o-s.
- Strong ($\Pi > 3\%$) and variable polarization.

1. BL LACs
- Observation: Flat, featureless($L_{balmer}/L_{edd} < 5 \times 10^{-4}$), $EW < 5 \circ A$. Opt.spectrum in high polarization.

2. FSRQ
- Observation: Opt.spectrum with features(quantitatively defined broad Balmer lines).
- subtypes: OVV and HPQ.
OVV: optical spectrum with features, stronger variability than BL Lacs, lower polarization.

4.2.5 LINERs

- Emission: narrow, low-ionization emission lines
- Continuum: Weak non-thermal continuum.
- HEG: Quasar, Seyfert; LEG: LINERs, absorption line quasars

5 AGN X-ray Emission

X-ray emission comes from a very limited region of AGN.

- 2 components:
  power-law cutoff continuum and reflection continuum
- 3 signatures:
  photo-electric absorption, Fe-Kα fluorescence lines, and Compton scattering hump
- Additional features:
  warm absorption and soft excess
- ionization parameter:
  1) Flux/density of the medium

$$\xi(r) = \frac{4\pi F_X}{n(r)} = \frac{L_X}{nR^2} = \frac{L_X}{N_H R}[\text{erg cm/s}] \qquad (61)$$

  2) $U = \frac{Q}{4\pi n_H r^2 c}$ $Q = \int_\nu^\infty L_\nu d\nu$

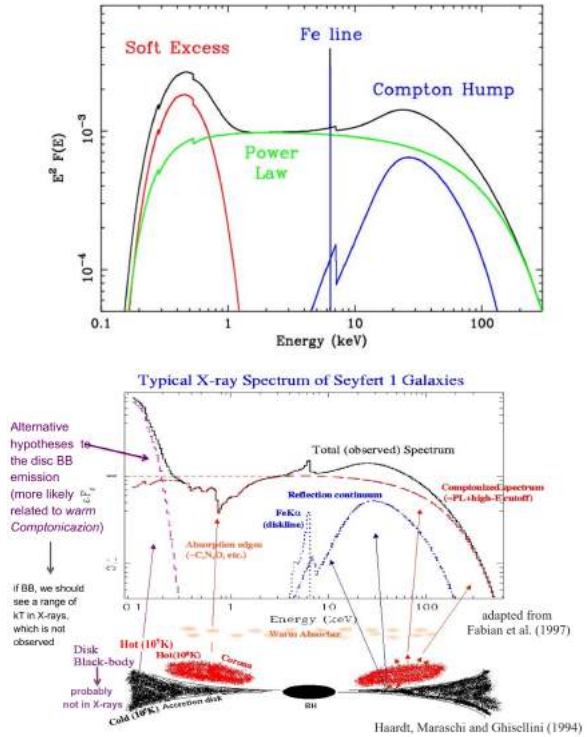

Figure 22: SED in X-ray: This figure indicates that we need a broad coverage of the telescope to cover all of the X-ray spectrum for analysis the features of AGN.

5.1 Thermal Comptonization hump

- Two-phase model: cold disc($T \sim 10^5 K$, B.B.) + hot corona($T \sim 10^8 K$, Comptonization, basically I.C.)
- Open issues for cornona: position, geometry, heating mechanism of cornona.
- Why the Comptonization in X-ray is thermal emission?
  Because the velocity e^- in corona follow a Maxwellian distribution. (Why??), aka $E_e \propto kT_e$.
- Cut-off: When $E_{cutoff} = kT_e$, the process of transfering energy is not efficient anymore.

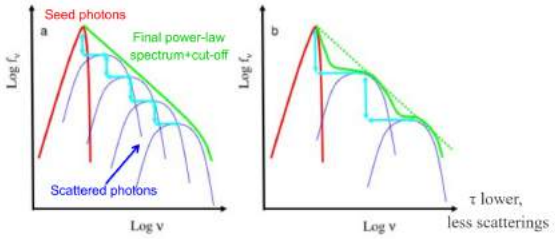

Figure 23: up-scattering photons and cut-off:
up-scattered photons become new seedsof comptonization. When up-scattering photons have the same energy with e^-comptonizaition are not efficient any more and the pwer-law cut-off is set up.

5.2 Reflection components

Half IC photons are directly observed by observers, half IC photons reflect into accretion disks and go through **another scattering process(IC/Thomson/Photoelectric Abosorption..)**
Typical features:

- Fluorescence lines
- Absorption edges
- Compton Hump ~30keV

5.2.1 continuum features in different bands

1. $< 10keV$: absorption edges
   - Primary X-ray emission interacts with circumnulear medium
   - Photoelectric cutoff $\Rightarrow$ indication of amount of obscuration materials
     $log(N_H) \sim 21, \tau_{opt} \sim 1$, absorption at $< 1keV$
     $log(N_H) \sim 24, \tau_{comp} \sim 1$, absorption at $< 10keV$
     In highly obscured AGNs, the soft X-ray emission can be totally absorbed.
   - Physical reason: E $\uparrow$, cross-section $\downarrow$: $\sigma \propto E^{-3.5}$. so the total optical depth is:

$$\tau_e(h\nu) = \int \sigma_e n_H dl = 2\times10^{-26} \left(\frac{h\nu}{1\text{keV}}\right)^{-\frac{8}{3}} \int n_H dl \qquad (62)$$

     For $\tau > 1$, $n_H \uparrow$, $h\nu \uparrow$.
     n_H: H-equivalent density of metal
   - soft X-ray emission is totally missed in highly-obscuration AGN. So it is a good way to distinguish Type 1/2 Compton thin/thick AGN.

- In optical/near-IR we 'talk' about dust extinction, in X-rays about gas absorption which is mainly due to metal.
- Depression of most fluorescence lines.

2. $\simeq 10 - 40keV$: Thomson Scattering. Compton Hump at 20-30keV.
3. $\geq 40keV$: K-N Effect but no Thomson scattering engine.
   Photoelectric absorption becomes important again.

5.2.2 Fe-Kα fluorescence line

1. Frequency: 6.4keV.
2. Relativistic profile
   The line is produced in the innermost region of AGN so we expect a broad shape affected by relativistic effect up to a few keV.
   - Doppler Effect: Double peaks
   - Special relativity: blue wing prominent
     $I_\nu = \sigma^3 I'_{\nu'}$
     $\sigma = \gamma^{-1}(1 - (v/c)cos\theta)^{-1}$: Doppler factor.
   - General relativity and transe doppler: Red wing prominent
     Gravitational redshift: $1 + z_{gr} = (1 - \frac{2GM}{c^2 R})^{-1/2}$
     R $\downarrow$, $z_{gr} \uparrow$, Fe lines extend to $\downarrow$ energies.

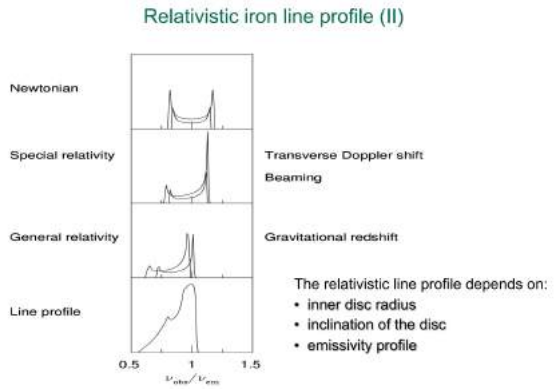

Figure 24: relativistic profiles

3. BH Spin: Measure BH spin based on Fluorescence lines + continuum information
4. factors that decide the shape of relativstic profiles:
   - inner disc radius: Schwazschild: $r = 6R_g$; Kerr: $r = 1.24R_g$. So Kerr BHs have broader profiles.
   - Inclination of disc:
   - Emissivity profiles:

$$\varepsilon(r) \propto r^{-q}$$

   $q \uparrow$,$\epsilon(r)$ closer to BH. $z_{gr} \uparrow$, the photons move to a lower frequency, and the low-frequency part of the line is higher.

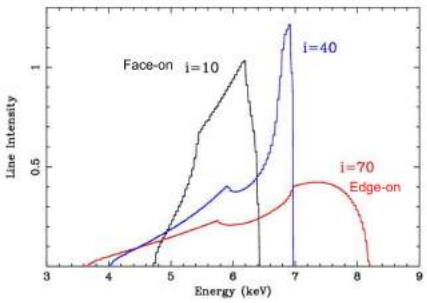

Figure 25: inclination of discs

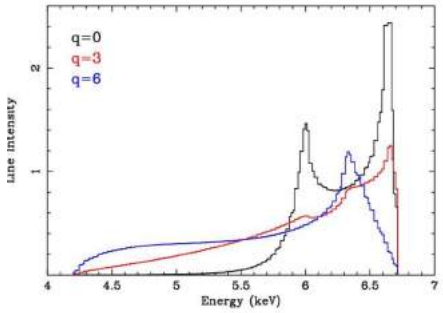

Figure 26: the shapes of profiles affected by emissivity

5.3 Warm Absorbers and UFO

1. Observation properties of WA:
   - Prominent ionized O edges($E \simeq 0.74(OVII) - 0.84keV(OVIII)$)
   - Found in 50% of Sey 1s.
     For TypeII objects, a lot of photons are going through photoionization, so it could be very challenging to observe the phenomena.
   - Blue-shifted spectra with $v \simeq 100 - 1000km/s$: indicates that it's blue-shifted wind from the accretion disc.

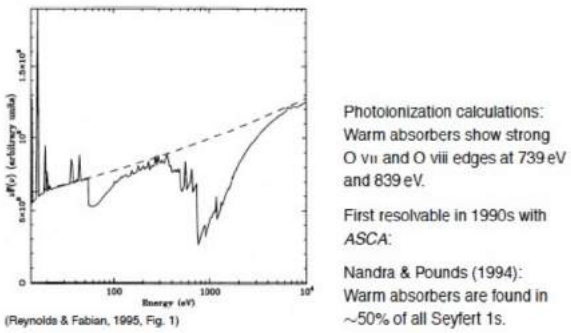

Figure 27: warm absorber

2. Observation properties of UFO:
   - $v \simeq 0.1 - 0.7c$

- Highly ionized($< log\xi >\simeq 4$, Fe^{25+}, Fe^{26+}) and large column density$< logN_H \simeq 23 >$

- Why it cannot be jets?
  The modeling shows it is wind but not jet since the physical properties are not consistent with jets in RL AGNs.
  Jets can have a few degrees of angle but winds can have angles of tens of degrees.

- approximation shows $\sim 50\%$ of local AGNs are with UFOs.

3. Unified Model:

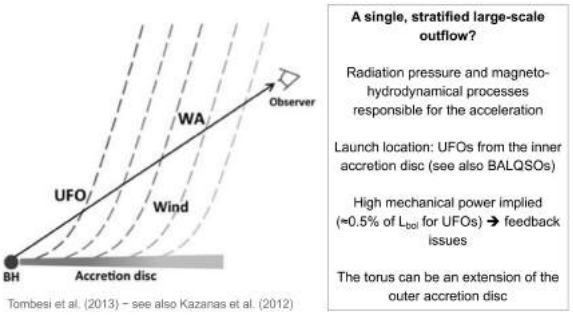

Figure 28: a single, stratified large-scale outflow

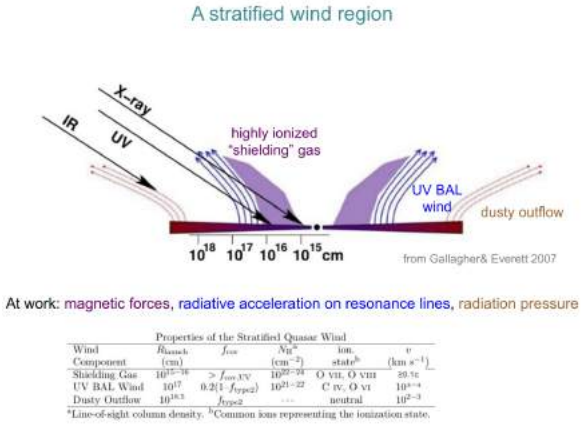

Properties of the Stratified Quasar Wind

Wind Component	R_{launch} (cm)	f_{ion}	N_H[a] (cm^{-2})	ion. state[b]	v (km s^{-1})
Shielding Gas	$10^{15.5-16}$	$> f_{ion,UV}$	10^{23-24}	O VII, O VIII	10-1c
UV BAL Wind	10^{17}	$0.2(1-f_{type2})$	10^{21-22}	C IV, O VI	10^{-4}
Dusty Outflow	$10^{18.3}$	f_{type2}	...	neutral	10^{2-3}

[a]Line-of-sight column density. [b]Common ions representing the ionization state.

Figure 29: The possible mechanisms of outflows in different scales

- Observation confirmation: $r-\epsilon$, $r-v_{out}$, $\xi-N_H$, $\xi-v_{out}$

- the issue of outflow unified model:
  1. Because of the acceleration process, we need something between the wind and radiation field to avoid the optical-UV spectrum being totally ionized.
  2. time-scale issue: Some Rg for ufo (10^{13} cm) outflows are on Kpc scales (10^{21} cm) when we divide by c to get a timescale we are obtaining thins different by several orders of magnitude, UFO are observed varying very fast outflow instead vary on extremely large timescales.

4. Calculate the model of outflows: Energy-driven or momentum-driven? Fig30.

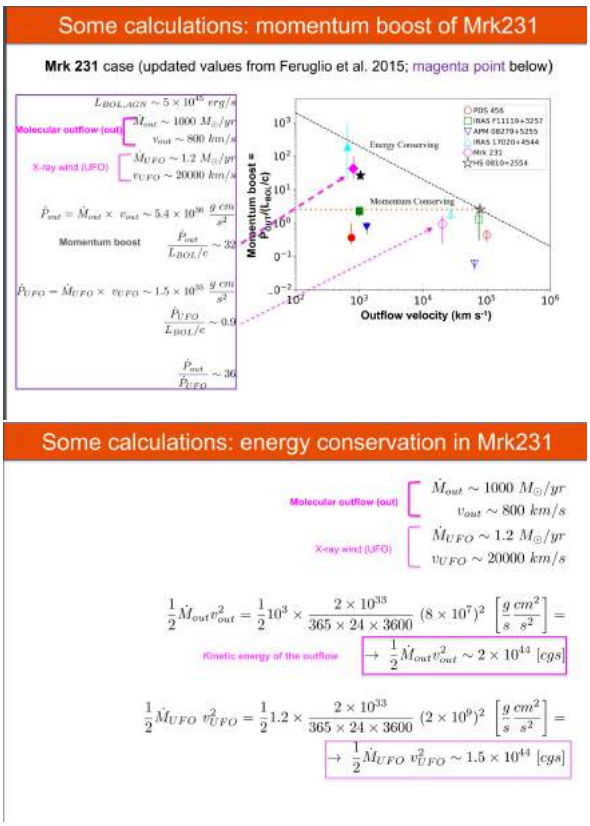

Figure 30: case of Mrk231, momentum rate, and outflow energy

5. X-ray binaries can also have UFOs.

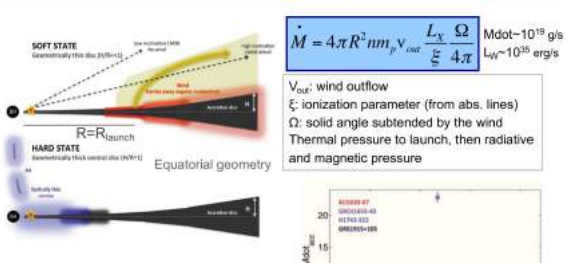

Figure 31: Models of winds in XB

5.4 Soft Excess

- Open issue: In the past $\Rightarrow$ high-energy tail of the thermal emission of the disk.

- In fact, the T of the disk should be nearly constant. ($kT \simeq 0.1-0.2keV$), regardless of the mass and luminosity of AGN.

6 AGN Radio Emission and Radio-loud AGN

6.1 Physical Classification

- In the quasar mode feedback mechanism, a large amount of gas flow falls inwards feeding the BH through an efficient SSC73 disc. This mode has an impact role in quenching SF and setting up $M_{BH} - M_{Bulge}$ relation.
  This mode can generate powerful radiative feedback and relativistic jets. The advance of the head of the jet generates lobes which are shocked regions of swept-back material or backflow. Hot spots are observed. Most of these RL AGNs are FRII/HREG galaxies.

- In the radio mode feedback mechanism, the material is accreted into the BH in a radiatively inefficient way (ADAF). The bulk of the energy is kinetic through radio jets.
  The jets decelerate and become sub-relativistic on scales of hundreds of pc to kpc. Most of these RL AGNs are FRI/LERG galaxies.

- comparison:

QUASAR MODE	RADIO MODE
Efficient Accretion	Inefficient Accretion
Standard SSC73 disc	ADAF accretion disc
HERG-FRI: jet dominanted, edge-darkened, jet scales: pc-kpc	LERG-Most FRII: moderately relativistic jets, lobe dominated, edge-brightened, scales: up to Mpc

6.2 Morphological Classification: FR I/FR II

- Why there are lobes?
  Jets terminates in the large lobes with a termination shock at its outermost edge.

- Why there is only one jet in FR II?
  Different doppler enhancement of the emission toward the observer.
  f_+: the observed flux of the jet approaching us
  f_-: a flux that from dimming for the receding jet
  $\beta = v/c$
  α: spectral index of observed continuum
  θ: angle of the ject with l.o.s

$$\frac{f_+}{f_-} = (\frac{1+\beta cos\theta}{1-\beta cos\theta})^{2+\alpha} \tag{63}$$

- estimation of jet speed:
  f_-: upper limit
  f_+, α: observables
  θ: assumed from the observed geometry

6.3 Jets

In powerful RL galaxies, we can probably observe extended jets structures to Mpc which are beyond galaxies (kpc).

1. Scale: Up to Mpc.

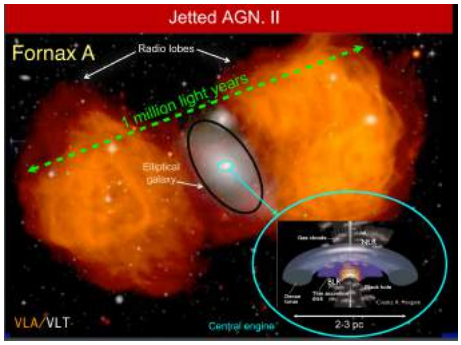

Figure 32: Scales of components in AGN

2. Features: extended synchroton emission, a lot of spatial components, spectral complexities. Jet power: $10^{45} - 10^{47}$erg/s to $10^{59} - 10^{61}$erg in lobes in 10^7years.

3. Formation of jets:

   - Energy source: the rotation of the BH.
   - Conditions: BH spins + magnetized accretion disc(twisting magnetic field lines $\Rightarrow$ extract rotational energy from the rotating BH).
   - Picture:

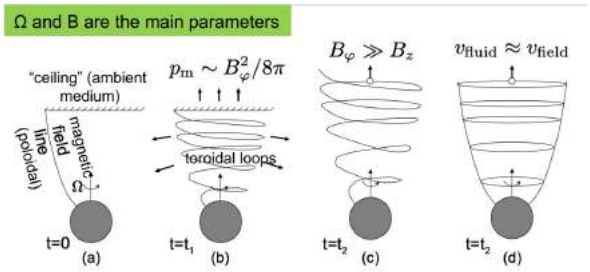

Figure 33:

4. Emission of jets: Synchroton.

5. Power function of jets:

$$P_{BZ} = \frac{k}{4\pi c}\Phi_{BH}^2\Omega_H^2 f(\Omega_H) \tag{64}$$

   for thick disks ($H/R \geq 1$): $P_{jet} \propto {\Omega_H}^4$

6. Doppler-boosted radiation in jets:

$$\begin{aligned} \delta(\beta,\theta) &= \frac{1}{\gamma(1-\beta\cos\theta)} \\ \beta &= \frac{v}{c} \\ \gamma &= \frac{1}{\sqrt{1-\beta^2}} \end{aligned} \tag{65}$$

The observed flux density modified by doppler-boosted radiation: The observed flux is extremely high in small

For an intrinsic power law spectrum: $F'(\nu') = K(\nu')^{-\alpha}$
the observed flux density is

$$F_\nu(\nu) = \delta^{3+\alpha} F'_{\nu'}(\nu)$$
$$\Delta t = \Delta t'/\delta$$

Figure 34:

angles, namely the jet emission is strongly boosted by a large doppler factor.

6.3.1 Jets in Blazars

1. Why the spectrum is featureless? The blazar objects are observed very closed to the jet axises.
   - No efficient accretion in this direction.
   - Degretion effect dominated by synchroton emission from Radio to Optical bands.
2. Double-peaked SED
   - First: IR ⇒ X-ray
   - Second: MeV ⇒ TeV
   - The difference of between Low-power and High-power BL lacs:

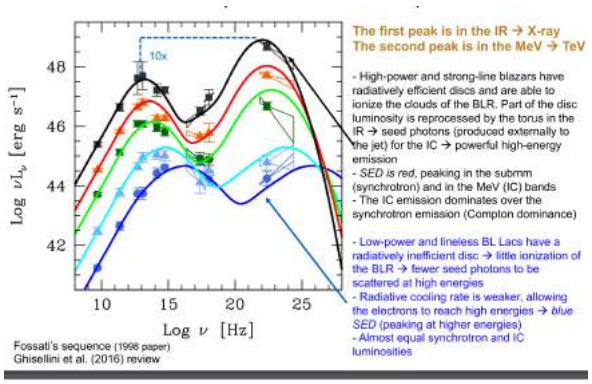

Figure 35: Red SED and Blue SED

- BL LAC: SSC; FSRQ: External IC with photons from discs/BLR, NLR/torus
  The difference between BL Lacs and FSRQs are in the second peak.
   - From EHBL to FSRQ:
3. Overall pictures with jets and inclination:

1) HERG: accretion disc and jet emission are in competition. Thermal radiation can be dominated from IR to X-ray. They can be FR II/FSRQ.

2) LERG: Non-thermal radiation from jets dominates the spectrum. AS inefficient accretion flows (ADAF), they can be BL FR I/BL LAC.

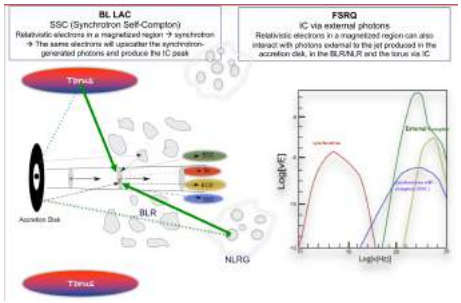

Figure 36: External IC

Abbreviation	Expansion	Probable radio parent	Emission lines
Extreme HBL	TeV blazars (BLL)	Low-luminosity FR-Is	Weak
HBL	High-energy peaked (blue) BLL	FR-I sources	Weak
IBL	Intermediate-energy peaked BLL	FR-I/II break sources	Weak
LBL	Low-energy peaked (red) BLL	Class B FR-IIs	Weak
FSRQ	Flat-spectrum radio quasar	BLRG, FR-II QSR	Strong

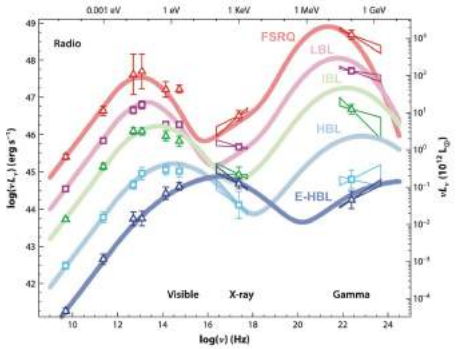

Figure 37: blazars with radio parents, double peaks for different blazars

3) Blazars are dominated by non-thermal radiation from jets.

6.3.2 Superluminal motions

[pro]
$v_\perp{}^{max} = v\frac{1}{\sqrt{1-v^2/c^2}} = v\gamma$ See Fig39

6.4 Equipartition

When the particle (electron and proton) is close to the magnetic field energy, the system is under equipartition magnetic field whcich can be an assumption to produce properties of radio sources. (?)
At frequency ν: $E \propto B^{-1/2}$
$\nu \propto E^2 B$

$U_{el} \propto B^{-3/2}$ *for a given synchrotron* L

$U_{tot} = U_{el} + U_{pr} + U_M = (1+k)U_{el} + U_M \propto (1+k)B^{-3/2} + B^2$

The total energy is minimized when :

$dU_{tot}/dB = 0$

$$\frac{\text{Particle energy density}}{\text{Magnetic field energy density}} = \frac{(1+k)U_{el}}{U_M} = \frac{4}{3} \tag{66}$$

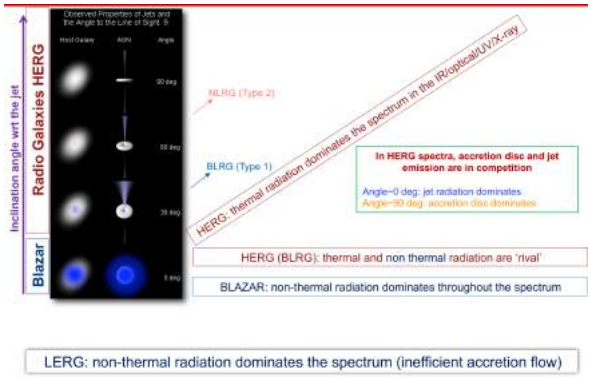

Figure 38: inclination with jets

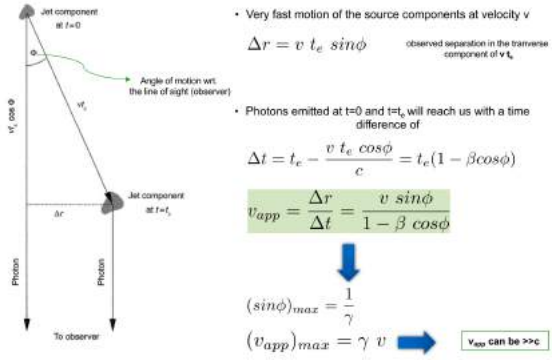

Figure 39: derivation of superluminal motions

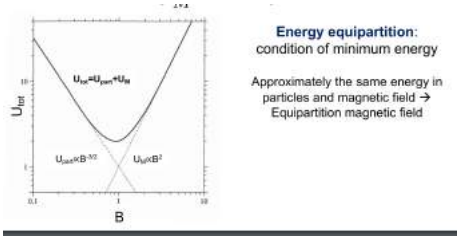

Figure 40: $U_{tot} = U_{part} + U_M$

7 AGN IR Emission and Obscured AGN

7.1 Models for AGN IR Emission

1. Smooth dust distribution Model

   - Dust grains around AGN. Obscuration ⇒ geometrical issues.

2. Clumpy models (More reliable)

   - dust grains in clouds. Obscuration(Type II AGN) can also happen at large inclination angles over equatorial plane.

   - The obscuration are more likely linked with the probably of the number of clouds at l.o.s.

   - Different T of dust coexist at the same distance.

   - Scheme from BLRs to torus: wind scenario

1) Clumps are pushed radially by the radiation of the central source

2) Dust is heated

3) IR radiation from the surrounding clumps

4) radiation force balances with gravity ⇒ keep the structure

5) $R < R_s$: dust-free, BLR Clouds; $R > R_s$: part of the torus.
   In disc outflow models, the division depends on central radiation field.

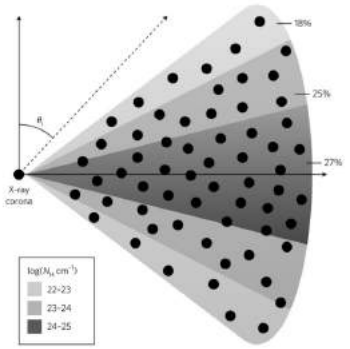

Figure 41: In clumpy models, the obscuration is more linked wtih the probability of the column density/number of clouds
It is possible that the column density along l.o.s. is different from the average column density of the torus. So SED fitting with proper X-ray models are needed.

3. outer radius of the accretion disc: self-gravity radius

   $$\mathrm{R_{SG}} \sim 0.04\mathrm{pc} \text{ in case of } \mathrm{L_{AGN}/L_{Edd}} \sim 0.1, 10^9 \mathrm{M_\odot BH} \quad (67)$$

   The the disc starts to fragment into clouds.

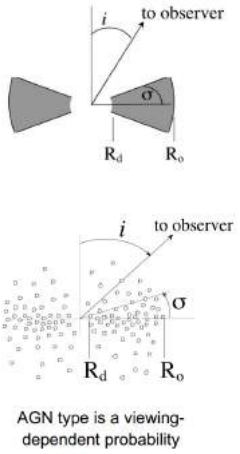

Figure 42: smooth distribution and clumpy model

4. Why clumpy model wins? What observational results support clumpy model?
   Correlation between absorption column density from X-ray spectra and the relative strength of Si line.

7.2 Sublimation Radius and Self-gravity Radius

1. Dust sublimation Radius:

   $$R_d \approx 0.5 L_{46}^{1/2} \left(\frac{1800K}{T_{sub}}\right)^{2.6} f(\theta) pc \propto L_{46}^{1/2} T_{sub}^{-2.6}$$
   $$R_d \approx 1.3 L_{46}^{1/2} \left(\frac{1500K}{T_{sub}}\right)^{2.6} f(\theta) pc \quad (68)$$

   Sublimation radius: outer boundary of BLR clouds and inner radius of the dusty torus. It determines where the torus starts.

2. Self-gravity Radius:

   $$R_{SG} \sim 1680 M_9^{-\frac{2}{9}} \alpha^{\frac{2}{9}} \left[\frac{L_{AGN}}{L_{Edd}}\right]^{\frac{4}{9}} \left[\frac{\eta}{0.1}\right]^{-\frac{4}{9}} R_g \quad (69)$$

   $R_{SG} \sim 0.04$pc in case of $L_{AGN}/L_{Edd} \sim 0.1, 0.1, 10^9 M_\odot$BH.
   The ouder radius of accretion discs.
   Both radii are linked with AGN luminosity. (Why linear?)

7.3 9.7μm Silicate Feature

1. Type 1/Type 2 diagnostic tool in IR band:
   Opt.depth of Silicate Feature at 9.7 μm.

2. Silicate Feature vs. X-ray obscuration
   Is the torus the same in terms of **geometry and physical properties** in mid-IR and X-rays?
   Not always. With different samples the results can be different.

- Confirmations: Systematic multi-wavelength study shows the N_H is the same in two bands. The SED

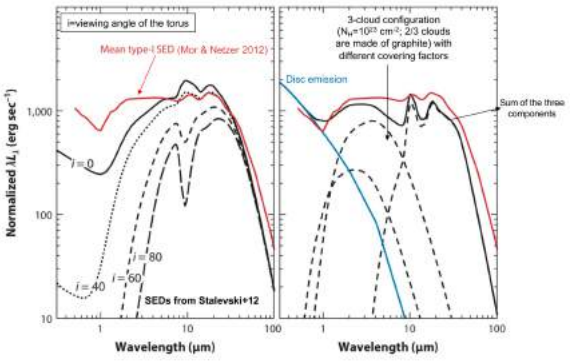

Figure 43: Silicate Feature from Type1 to Type2.

fitting with three components (host with young and old stars, AGN and SF regions which extended to far-IR due to the cold dust 30K emitting like a gray body) also supports that.

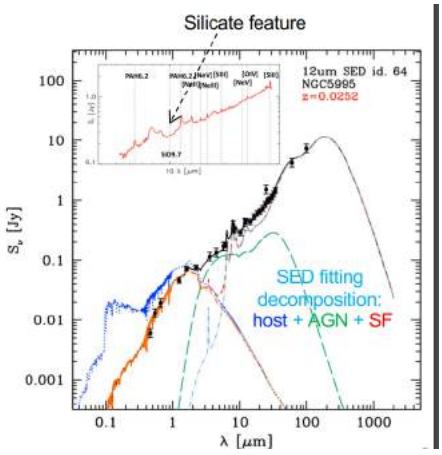

Figure 44: SED fitting with multi-wavelength data

- Doubts: Compton-thick AGNs with Little Apparent Dust Extinction
  There are a few CT AGN sources with high column density($> 10^{24}$) but with almost no Si absorption. Aka "True" Type-II AGN. It means the obscuration cannot only depend on torus. It is also possible that host galaxies participate into obscuration (disturbance, dust lanes etc.).

7.4 Properties of Obscured AGN

1. Definition

- Obscuration = function of opt.depth, covering factor, etc.
  Cannot observe the emission from accretion disk due to the obscuring materials.

- **Classical definition**: absence of BLR emission in optical bands.
  absorbing column density $N_H > 10^{22} cm^{-2}$ measuring in X-ray band

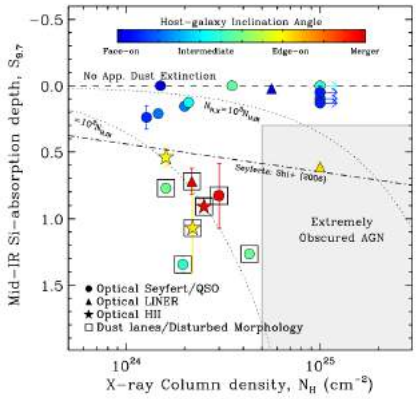

Figure 45: Compton-thick AGNs with Little Apparent Dust Extinction

Unobscured AGN: BLR emission + NLR emission ($N_H < 10^{21} cm^{-2}$)
obscured AGN: NLR emission

- **Compton-Thick AGN**: ($N_H > 1.5 \times 10^{24} cm^2$) are the most heavily obscured class of AGNs; they are extremely difficult to detect and remain hidden in most X-ray surveys
  Conclusive identifications of Compton-thick AGNs are made through spectroscopic X-ray observations performed at E > 10 keV, where the relatively unabsorbed high-energy emission can be directly detected.

2. Covering factor: can be estimated using SED fitting with multiple (host, AGN, SF regions) components. For clumpy models, it depends on the number of clouds at l.o.s.

3. Dust: absorption in UV-IR bands. Gas: absorption in X-ray bands.

4. Mid-IR to optical time lags: $\Delta t \propto L^{0.5}$

5. CT AGN at High-z:

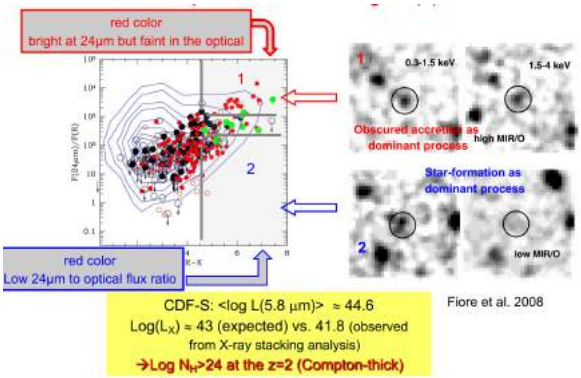

Figure 46: optical/mid-IR selection of high-z CT AGN

7.5 Mechanism of obscuration

1. The nuclear torus and the unified model
   Clumps in the torus obscured BLRs and inclination of AGNs are taken into accounted.

2. Obscuration by a nuclear starburst/disturbed morphology

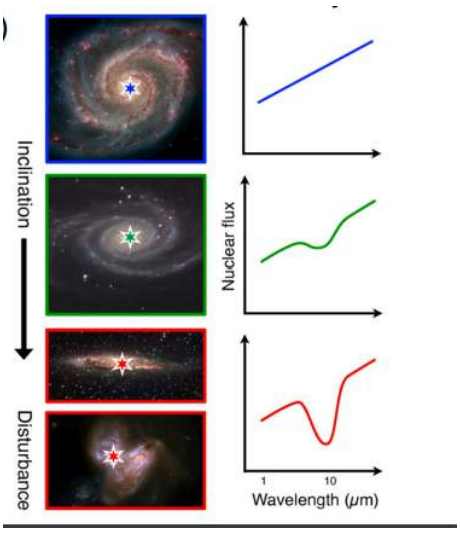

Figure 47: Morphology contribution

3. Obscuration by galactic materials

- dust lanes: the medium inside host galaxies can provide obscuration.

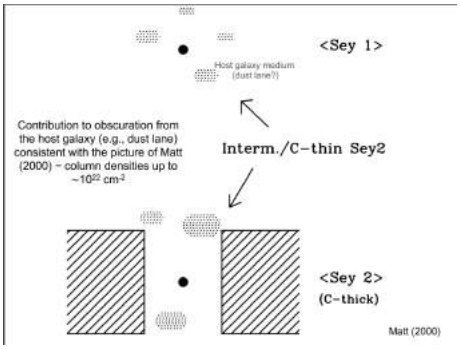

Figure 48: Dust lanes can produce C-thin Sey2.

- Cloudy model of BLR: Obscuration as a transient event
  X-ray sources are eclipsed by some absorbers made of BLR clouds, which transiently changes the N_H. The absorbing clouds may have a comet-like structures.

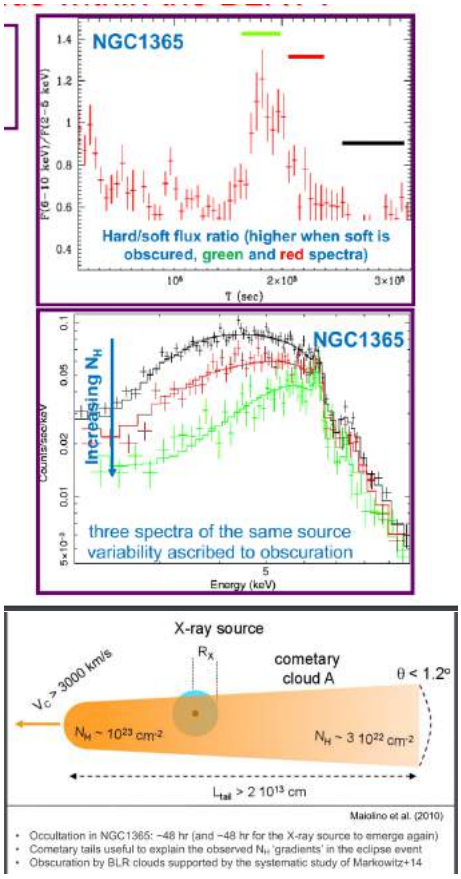

Figure 49: $\Delta H \sim 10^{23} - 10^{24} cm^{-2}$

8 AGN Surveys and Selections

Completeness (low biased, how many AGNs can be selected with this methods-100%) vs. reliability issues (contamination, how many fake sources are selected)

- raido with $f_r \leq 1mJy$: we can select a lot of radio galaxies including both RL and RQ AGN; the bias is low because there is no obscuration in radio bands. Contanimation is from star-forming process.
- Same as mid-IR: It is very powerful with weak obscuration bias but with somehow contanimation from SF. (e.g. PAH lines from star-forming galaxies)
- optical selection: it is highly efficient and with high reliability for type1 AGN. But it is not complete because of the losing most of obscuration AGN. Contamination is from the host galaxy.
- X-ray: Can detect a significant number of Type 2 AGN. Completeness is weak for low-luminosity sources such as obscuration AGN at high-z.
- γ-ray: non-jetted sources are losing.
- Variability: low efficiency because of long-term monitoring.

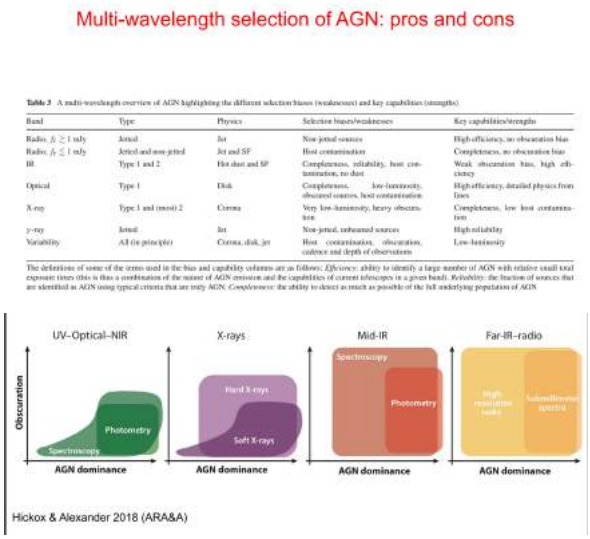

Figure 50: individual bands selection: In particular, photometry data is limited but easy to peak. For limited observation time it is better and easier. In general spectroscopy data is better

8.1 Multi-wavelength signatures of AGN

See Fig 51

1. bottom right: unobscured powerful type I AGN:
   - optical/uv: big blue bump which is the peak of accretion discs
   - X-ray: emission from comptonizaiton continuum and some hot gas + binaries.
2. up panels: emission from accretion discs are disappered.
   - Contanimation: Radiation not from AGN are contanimation of observations. In up panels they can be from binary stars or supernova.

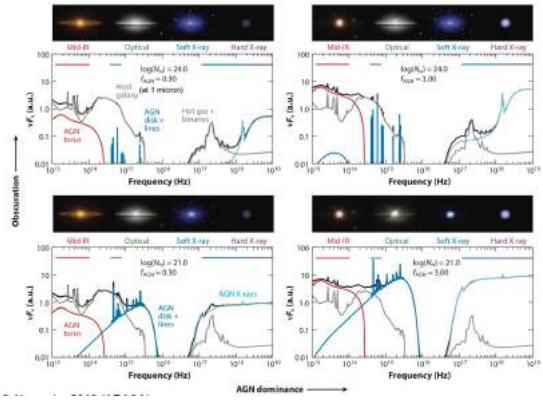

Figure 51: Multiwavelength signatures of spectrum

8.2 AGN surveys for obscured AGNs

- X-ray gives you the indication of the amount of obscuration and how powerful the AGN it is.
- SED fitting is important to show the presence of AGN.

8.2.1 Criteria used for Obscured AGN selection

See Fig52

8.2.2 Multi-band selection methods

1. **X-ray wide-adopted method**
   - flat observed photon index $\Gamma < 1$. Unobserved with $\Gamma > 1.8$. Con: With low resolution/limited photometry points it is possible to fit data with index < 1.
   - Strong $Fe - K\alpha$ line ($EW > 1keV$).
   - Hardness ratio $HR = (H - S)/(H + S)$ From -1 to +1.
2. **Mid-IR + Optical selection + X-ray Stacking**
   - Mid-IR-bright: For obscured AGNs, mid-IR emission is due to reprocessing of intrinsic AGN emission.
   - UV/optical-dimmed: emission is extincted but reemerges as IR emission.$F(24\mu m/F_R) > 1000$
   - X-ray stacking image: In combination With mid-IR photometry data, stacking X-ray emission and consequent comparison with expected X-ray emission provides an estimate on the amount of obscuration

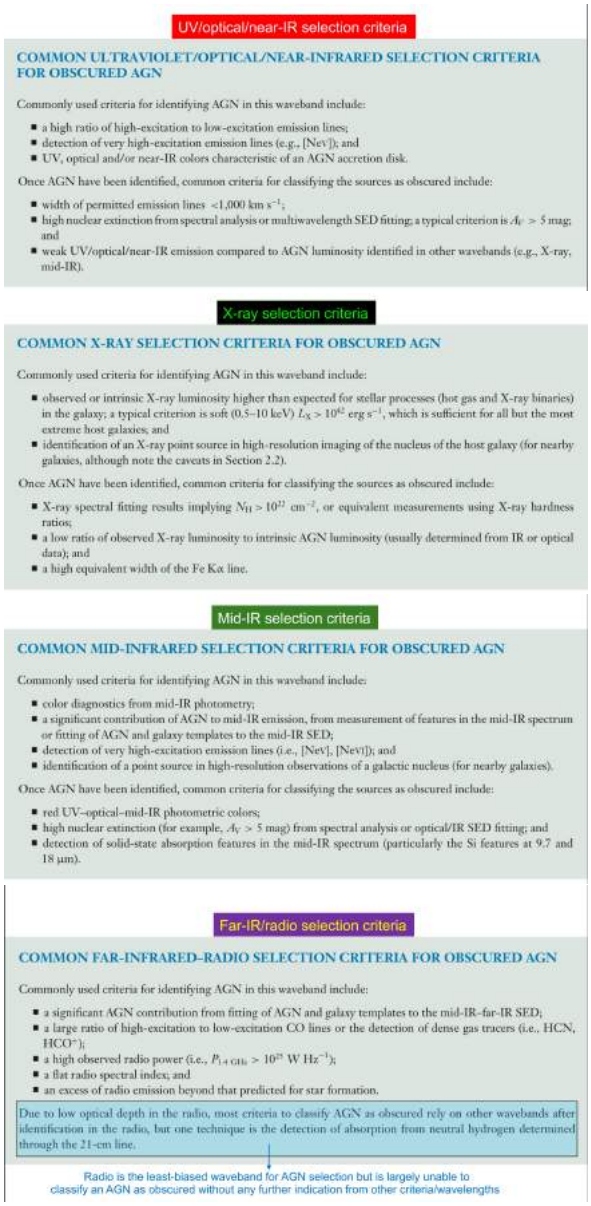

Figure 52: Multi-wavelength selection criteria

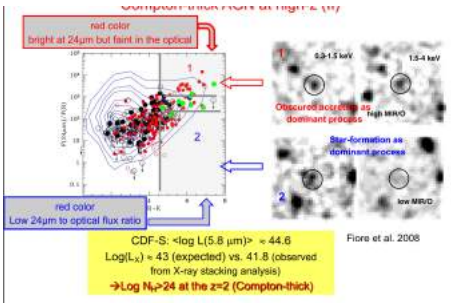

Figure 53: box 1 is obscuration AGNs with high MIR/O, box 2 is due to SF process.

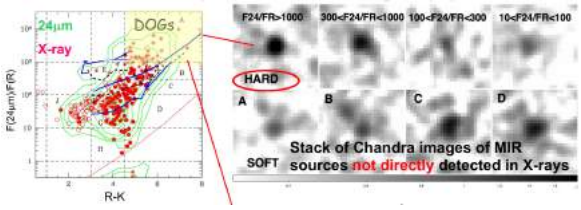

Figure 54: Dust Obscured Galaxies(DOGs) selection: X-ray confirmation for sources with different F24/FR

$F(24\mu m/F_R) > 1000$. Faint in opt., strong in mid-IR(AGN torus). See Fig5454

3. **Opt./IR + X-ray spectroscopy**

- Silicate Absorption + X-ray spectra(absorption in soft X-ray band)
  AGN presence: $[NeV]14.3\mu m, [NeV]24.3\mu m, [OIV]25.9\mu m$
  Low-resolution spectroscopy is enough but host galaxy also contribute into the absorption
  A clean view of photoionization from the nucleus.
- Color selection in mid-IR coverage. See Fig55

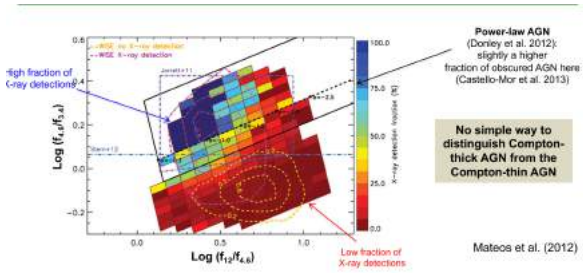

Figure 55: color selection

4. **Optical selection (up to $z \sim 1.5$)**

- OIII: Up to $z \sim 0.8$
- NeV:$L_X/L_{[NeV]} < 15$. Based on simulations, overall 43% of AGN are CT AGN. (?)
- From low to high-redshift using [OIII], [NeV] (fig57) and CIV lines (CIV: narrow component) and derive the space density of heavily obscured AGN.
  X-ray used to derive the amount of obscuration materials.

5. **Far-IR/millimeter selection**

- Molecules:
  dense ($n_e > 10^4 cm^{-3}$) molecular gas tracers (cloud cores, fuel for SF and possibly AGN): HCN, HNC, HCO+, CN are radiatively excited by mid-IR photons and can reveal the presence of obscured AGN.
  $HCN/HCO^+, J = 3 - 2$
  LIRG: the infrared emission is much more than star forimg galaxies which indicates that the IR emission is probably from the AGN activity. LIRG can be probed using the ratio.

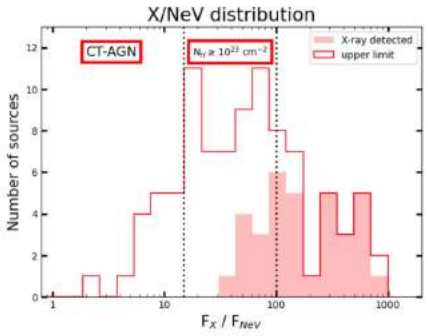

Figure 56: [NeV] Selection

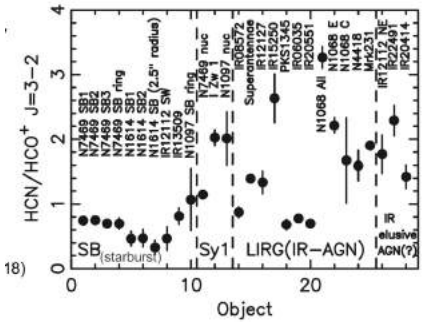

Figure 57: LIRG has higher line ratio than starburst galaxies.

- CO spectral energy distribution (COSLED): (up to $z \sim 6.4$). A high ratio of high-excitation to low-excitation CO lines (CO-excitation ladder) can indicate heating from an AGN.

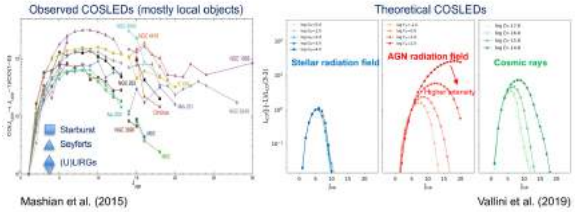

Figure 58: Theoretical COSLED depends on N_H and Temperature.

- Search for ULIRG/highly obscured AGN with k_{bol}: $k_{BOL} = L_{BOL}/L_{2-10keV}$, e.g. Chandra deep Field See Fig59.

8.3 AGN selections for high-z($z > 6$) AGNs

1. Drop-out Technique

- Condition: $i - z > 2$ at birght mags return unobscured AGN.Figure60.
- Contamination:
  late-type stars: similar i-z color but redder z-J/Y color.
  cool Dwarfs (T<3500K): similar color but surface density is 15x than QSOs.

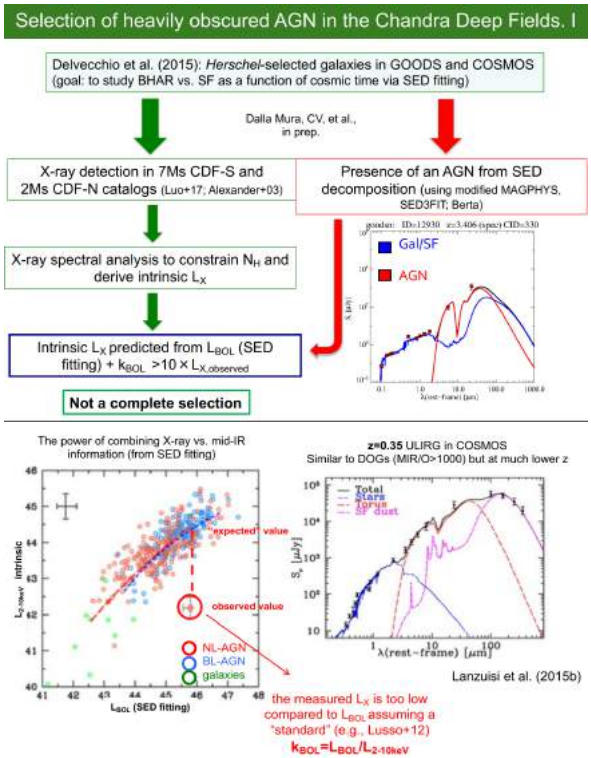

Figure 59: CDF selection procedures for ULIRG

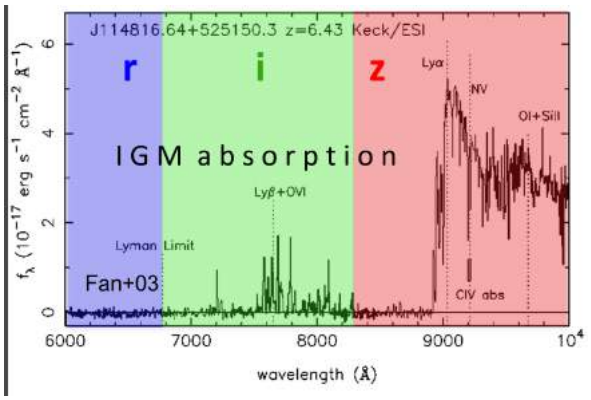

Figure 60: color selection

- Lyman-break galaxies (LBG)
  All of the photons at $\lambda < 912A$ are abosorbed by neutral H in IGM of galaxies themselves and the IGM on l.os. $\Rightarrow$ Lyman-break.

- Lyman-α emitters (LAE)
  Highly-redshifted $Ly\alpha$ lines excited by the UV light from young stars in ISM.

8.4 Strategies for AGN X-ray surveys

See fig61.

1. Large-area and deep-area surveys.

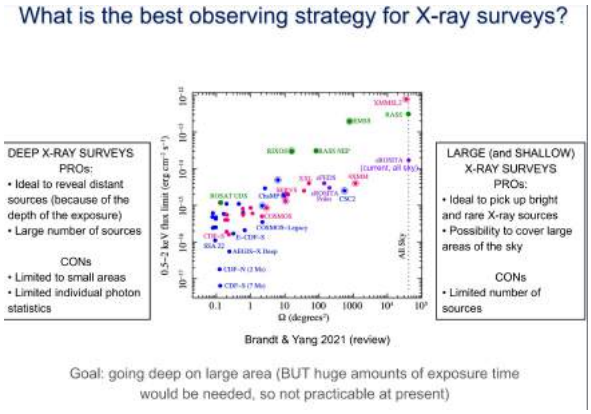

Figure 61: Two kinds of surveys

9 AGN Evolution and High-z AGN

9.1 AGN Luminosity Function and Scaling relations

1. Scaling relation: $M_{BH} - \sigma$ relation

- Scaling relations are the relations between BH mass and host galaxies properties(M_{bulge}, L, σ).
  The scaling relations show that AGN and host galaxies are closely tied for co-evolution.

- $M_{BH} \propto \sigma$ Intrinsic explanation: Balance between

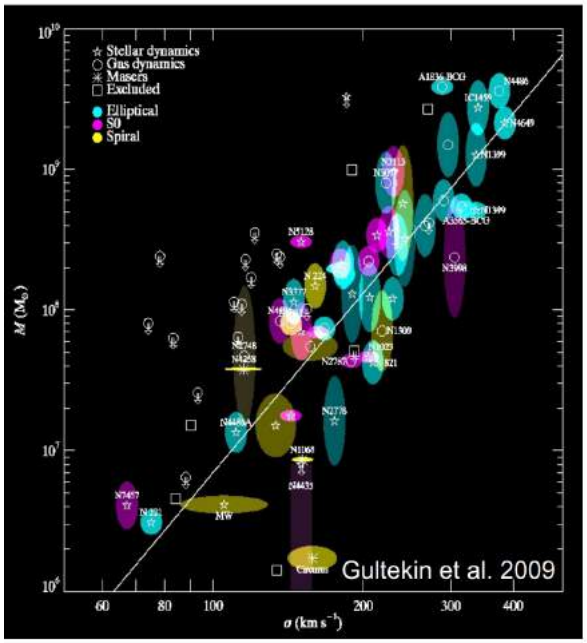

Figure 62: linear relation between BH mass and velocity dispersion

AGN activities($L_{edd} \propto M_{BH}$,tend to expel gas) and galaxy gravitational attraction ($E_{gr} \sim \sigma^4 R_e$, tend to retain gas). The balance is found for $M_{bh} \sim 10^{-3} M_{bulge}$,

2. AGN Luminosity Function

$$N(>S) = \int \frac{\Omega}{3} r^3 \phi(L) dL = \frac{\Omega}{3(4\pi)^{3/2}} S^{-3/2} \int L^{3/2} \phi(L) dL.$$
$$\phi(L,z) = f_{\rm d}(z) \phi\left(L/f_{\rm l}(z), z=0\right) \quad (70)$$

AGN L-dependent Density Evolution:
⇒ Similar to galaxies' downsizing mode. Figure63.

- Luminosity evolution: The density of the most luminous AGN peaks earlier in cosmic time than for less luminous objects. which implies:

- Density evolution: Large BHs are formed earlier than their Low-mass counterparts.

- Similar to galaxy evolution downsizing scenario: massive galaxies tend to form stars earlier and faster than less massive galaxies

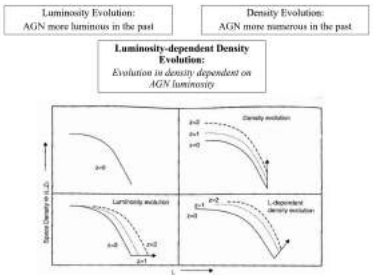

Figure 63: AGN LF evolution in cosmological scale

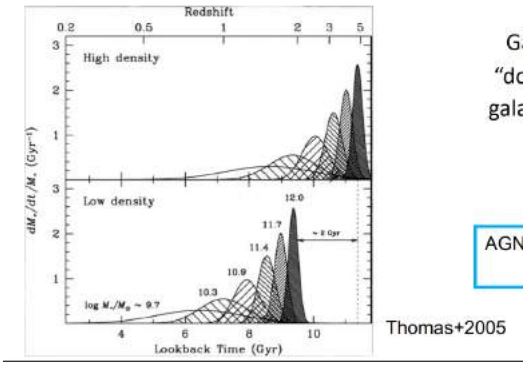

Figure 64: downsizing scenario

3. Soltan argument: estimation of BH mass density

- photon-counting exercise: every photon radiated by an active BH during the history of the Universe represents a certain amount of grams of SMBH mass today

$$u = \int_z^\infty \frac{dt}{dz} dz \int_0^\infty \Phi(L,z) L dL$$
$$\rho_{BH} = \int_z^\infty \frac{dt}{dz} dz \int_0^\infty \Phi(L,z) \frac{1-\eta}{\eta c^2} L dL \quad (71)$$

u: Integrated energy density from all AGN.
ρ_{BH}: Mass density of BH remnant.

$$u = \int_0^\infty dz \int_0^\infty dL \Phi(L,z) L \left|\frac{dt}{dz}\right| \sim 1.3 \times 10^{-15} \mathrm{ergcm}^{-3}$$
$$\rho_u = \frac{1-\eta}{nc^2} u \sim 2.2 \times 10^5 M_\odot Mpc^{-3} \quad \text{assuming } \eta = 0.1$$
Local mass density $\sim (3.5 - 5.5) \times 10^5 \mathrm{M}_\odot \mathrm{Mpc}^{-3}$ (72)

9.2 AGN Formation and Evolution

9.2.1 AGN and Galaxy co-evolution modes

1. The cosmic cycle of AGN and galaxy evolution:

- The galaxy mergers between gas-rich galaxies drive gas fuel in both SF and QSO activities, which obscured growth. (ULIRG, sub-mm phase). fig65

2. Two modes of AGN-GALAXY Evolution based on accretion modes:

- Luminous AGN: Mergers ⇒ obscured AGN ⇒ luminous quasars

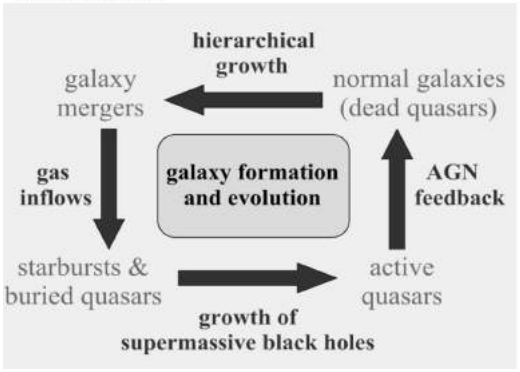

Figure 65: BH-GALAXY evolutionary cycle

- Low L AGN: Secular (disk instabilities, bars, minor mergers) ⇒ Low-L AGN, it's no need to have such a high rate of mergers.

3. BH-GALAXY evolutionary model: Figure66
   Example from gas-rich galaxy to luminous AGN:

1) **gas-rich galaxies–Mergers/ULIRG–Obscuration QSO**:
   gas-rich galaxies merge with each other. The strong galactic interactions produce a significant star-forming process. The gas inflows to fuel QSO activities generate obscuration.

2) **obscuration QSO–Unobscuration QSO**:
   When the QSOs reach accretion peaks, strong feedback is generated to blow out the gas making QSO unobscured. The objects are namely optically visible Broad-line AGNs.

3) **Unobscuration QSO–Transition objects (green valley galaxies)–passive rad galaxies/ellipticals**:
   The strong AGN feedback will probably quench the star formation process in host galaxies, the objects are in slow accretion and turn to passive red galaxies/ellipticals.

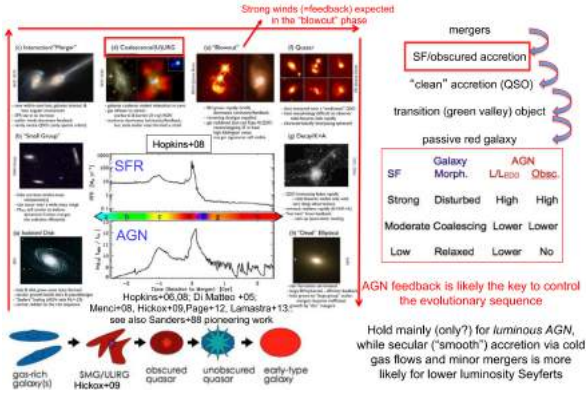

Figure 66: BH-GALAXY evolutionary model

4. Cosmic SFR associated with AGN Accretion (BHAD):

- cosmic noon: At redshift $z \sim 2-3$, the universe reached "cosmic noon", in which cosmic SFR and AGN accretion reached peaks.

- Importance of surveys for AGN evolution: To reconstruct both curves which have similar behaviors, it is necessary to have a complete AGN population sample as a function of redshift.

9.2.2 Cosmic x-ray background

- [PRO]Why XRB cannot be diffuse plasma emission?
  No compatible Brems. emission.
  IC effect produces distortion in hot gas($T \sim 40keV \sim 4\times10^8K$.
  CMB presents a perfect black body.

- the sources of XRB: Unresolved, fainted x-ray sources ⇒ AGNs.

- Spectrum of cosmic XRB: Fitting with the sum of obscured and unobscured AGNs.

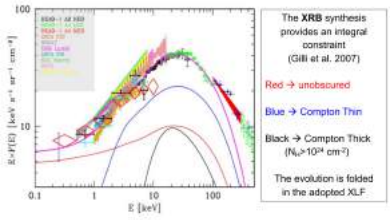

Figure 67: spectrum

- importance of XRB: The XRB records the accretion history onto SMBHs across cosmic time (i.e., is the integrated emission of AGN and quasars at all luminosities and redshifts).
  Besides a lot of problems, the observed density of BHs in the local–remnants of active galaxies–is consistent with XRB intensity.

9.2.3 Properties of High-z AGN

- Massive $M_{BH} \simeq 10^8 - 10^{10}M_\odot$. $L_{bol} \simeq L_{edd} > 10^{46}erg/s$.

- Metallicity: high-z QSOs are similar to low-z QSOs. SED is similar to low-z QSOs.

- SFR: Significant star formation at high-z:
  1. 30% high-z QSOs are detected at sub-mm/mm.
  2. luminosity and SFR:

$$L_{FIR} \approx 10^{13}L_\odot, T \approx 30{-}50,\ \mathrm{K}, SFR \simeq 1000M_\odot/yr \tag{73}$$

- BH mass: BH mass of high-z QSO are larger than expected of local $M_{BH} - M_{host}$ relation.

$$\mathrm{M_{BH}} \sim 10^9\mathrm{M_\odot} \rightarrow \mathrm{M_\star} \sim 10^{11}\mathrm{M_\odot} \rightarrow \mathrm{M_{halo}} >\sim 10^{12}\mathrm{M_\odot} \tag{74}$$

  It indicates that BH at high-z grows faster than the host galaxy.

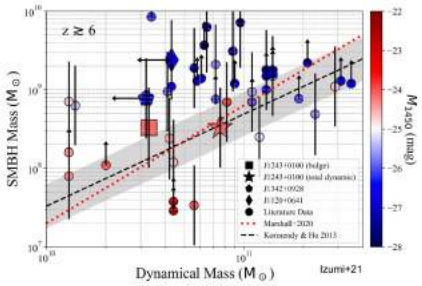

Figure 68: BH mass-dynamical mass

- Luminosity function for high-z QSO:
  High-z QSO flattened the faint-end slope of the LF meaning the number of AGN decreases at high-z. It indicates that AGN cannot contribute significantly to the reionization unless most of the population is missed.

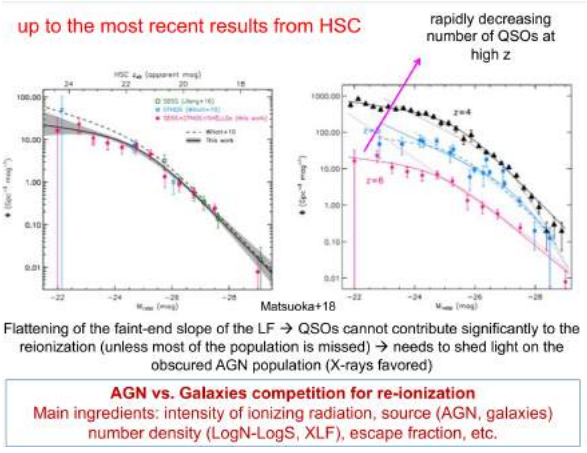

Figure 69: luminosity function of AGN

- AGN feedback at high-z:
  Massive outflow of [CII] $158\mu m$ line, of $\dot{M} > 3500 M_\odot/yr$ SFR in the host galaxy delected from Maiolino+12, Valiante+12.

- X-ray properties: fig70
  a steeper photon index due to on average high Eddington ratio. $\Gamma \simeq 1.6-2.4$.(Remind: $f_v^{-\alpha} = v^{\Gamma-1}$.)
  1. $z = 2-6$: The photon index doesn't change from z=2 to above 6, which means the small-scale X-ray emission regions of AGN appear to be insensitive to changes of z.
  2. $z > 6$: a steeper photon index due to on average high Eddington ratio.

9.3 BH seeds and BH growth

1. BH growth at high z: Super-Eddington accretion

$$M(t) = M_0 e^{\left(\frac{1-\varepsilon}{\varepsilon}\frac{t}{t_{\rm Edd}}\right)} \tag{75}$$

- BH seeds requires Eddington accretion ($\lambda_{edd} = 1$) for a quite long period (z=20). Rapid spinning BHs($\epsilon > 0.1$) cannot grow up to Supermassive BHs.

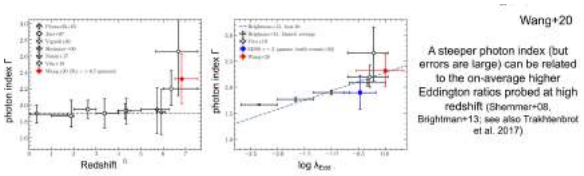

Figure 70: photon index linked with λ_{edd}, might be a way to calculate BH mass

- Super-Eddington accretion:
  Radiatively inefficient highly accreting BH (slim disk) provides fast growth.
  1. Radiatively inefficient
  2. Super-Eddington accretion

- BH Seeds see fig71

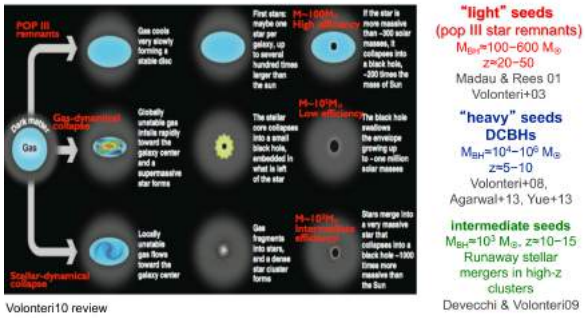

Property	Known $z \sim 5-7$ quasars	"Typical" AGN / galaxies
Luminosity, $L_{\rm bol}$ Obscuration / selection	$\gtrsim 10^{46}$ erg s^{-1} un-obscured / UV-opt.	$\lesssim 10^{45}$ erg s^{-1} ~50% obscured / X-ray
SMBH mass, $M_{\rm BH}$ Accretion rate, $L/L_{\rm Edd}$ Accretion mode	$\sim 10^9\ M_\odot$ ~ 1 thin disk, $\eta \gtrsim 0.1$	$\sim 10^7\ M_\odot$ $\sim 0.01-1$ (who knows, really?)
Implied BH seeds	massive, $M_{\rm seed} \sim 10^{4-6}\ M_\odot$	stellar (pop-III), $M_{\rm seed} < 10^3\ M_\odot$
Host mass, $M_{\rm host}$ Host SFR	$\sim 10^{10-11}\ M_\odot$ $\sim 100-3000\ M_\odot\ {\rm yr}^{-1}$	$\sim 10^{9-10}\ M_\odot$ $< 100\ M_\odot\ {\rm yr}^{-1}$
Large-scale env.	over-dense, mergers, outflows	"normal"?
Demographics	rare! $\Phi \lesssim 10^{-7}$ Mpc^{-3}	common? $\Phi \gtrsim 10^{-5}$ Mpc^{-3} (~10% of galaxies? less?)
Future prospects	*Euclid, Athena, WFIRST*	*Lynx*

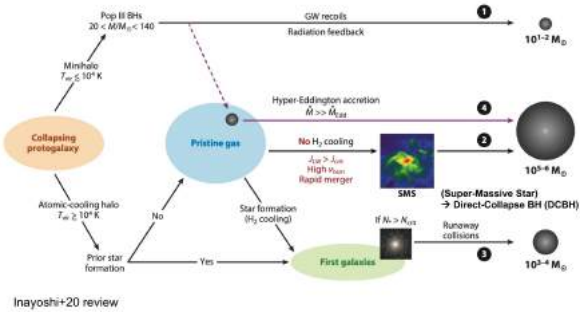

Figure 71: BH Growth model and properties of High-z AGN

9.4 High-z($z > 3$) Obscured AGN in X-ray surveys

Obscured AGN fraction increases with redshift, especially at high luminosity.

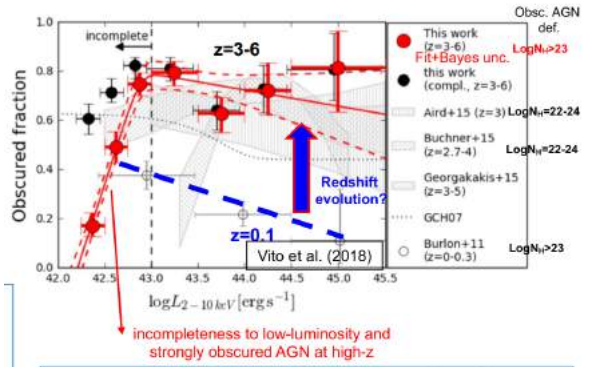

z>3 AGN: ≈70−80% with $N_H>10^{23}$ cm^{-2}
see also Iwasawa et al. (2012) – CDFS, 3Ms, z=1.7−3.7

Obscured AGN fraction increases with redshift, especially at high luminosity
More gas available, more mergers, …

On the realm of high-redshift AGN: a summary

- Where do we stand?
- Detection and identification of z≈6 QSOs is challenging because they are rare
- Luminous unobscured QSO properties currently known: SED, X-ray emission, metallicity and M_{BH} similar to lower-z QSOs
- Still missing the heavily obscured AGN at the highest redshift. Deep X-ray stacking limits the contribution of accretion in low-mass galaxies. Huge discovery field for next-generation facilities (but SHELLQ is promising)
- ALMA and NOEMA fundamental to place constraints to neutral/molecular gas, and the occurrence of feedback/outflows. Role of molecular gas in obscuration
- What are the progenitors (seeds) of high-redshift AGN? Where and when did they form? How z=6 SMBH preceded galaxy formation?
- We need large number of AGN to constrain models (beyond degeneracies) and physics at high redshift, and good photon statistics to characterize them

Discovery space for z>5−6 AGN and QSOs is huge

Figure 72: obscuration AGN at high-z

10 AGN Feedback

10.1 Relations in AGN Feedback

$$E_{BH} = \eta M_{BH} c^2 \sim 0.1 M_{BH} c^2 \sim 2 \times 10^{61} M_8 \ erg$$

Energy release via accretion

M_8 = BH mass in units of $10^8\ M_\odot$

$$M_{BH} \sim 2 \times 10^{-3} M_{bulge}$$

from local relations

$$E_{bulge} \sim M_{bulge} \sigma^2 \sim \frac{M_{BH}}{2 \times 10^{-3}} \sigma^2 = 4 \times 10^{58}\ M_8\ \sigma_{200}^2\ erg$$

Binding energy of the bulge

σ_{200} = velocity dispersion in units of 200 km/s

$$E_{gas} = f_g\ E_{bulge}$$

f_g = cosmological baryon fraction = $\Omega_B/\Omega_M = M_{gas}/M_{tot} \sim 0.16$

Binding energy of the gas in the bulge

$$\frac{E_{BH}}{E_{gas}} \sim \frac{2 \times 10^{61} M_8}{6.4 \times 10^{57} M_8 \sigma_{200}^2} \sim 3000\ \sigma_{200}^{-2}$$

Figure 73: $E_{acc} >> E_{binding} \Rightarrow$Feedback

$E_{accretion} >> E_{binding}$: The AGN can have a profound impact on the host but it should be inefficient to avoid disrupting galaxies.

10.2 Two modes of AGN Feedback

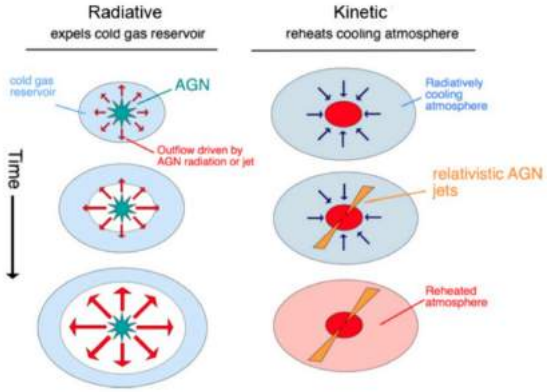

Figure 74: two modes

10.2.1 Radiative/Quasar Mode

- $R_{edd} > 0.01$, high-L AGN
- wide-angel winds driven coupling of radiation to the ambient medium
- hot thermal wind
- outflow rate:

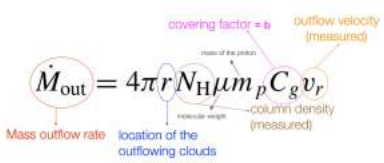

Figure 75: $\dot{M}_{out}$

- if close to Eddington limit:

A. **momentum-driven outflows**:

- Feature: only transfer momentum/ram pressure, thermal pressure is negligible. Significant cooling.
- Luminosity and Energy: $L_{BH,Wind} \sim 0.05 L_{edd}$
  Energy injected into the bulge ISM in the momentum-driven limit: E_{mom}

$$\dot{M} v \sim \frac{L_{Edd}}{c} = \eta \dot{M}_{Edd} c$$

$$\dot{m} = \frac{\dot{M}}{\dot{M}_{Edd}}$$

$$L_{BH,wind} = \frac{1}{2} \dot{M}_W v^2 = \frac{L_{Edd}}{c} \frac{v}{2} = \frac{\eta}{2\dot{m}} L_{Edd}$$

$$\sim \frac{\eta}{2} L_{Edd} \sim 0.05 L_{Edd}$$

$$L_{BH\ \text{wind}} \sim 0.05 L_{Edd}$$

$$E_{mom} \sim \frac{\sigma}{c} E_{BH,wind} = \frac{\sigma}{c} \frac{\eta}{2} M c^2 \sim 5 \times 10^{-5} M c^2 \sim 0.1 E_{gas} \quad (76)$$

- Scale: confined within ~ 1 kpc for I.C. cooling. Radiatively free-free cooling can extend farther away.

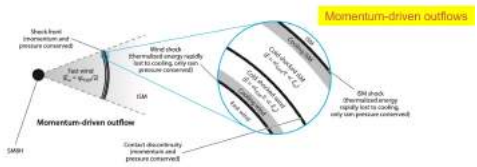

Figure 76: shocks of momentum-driven outflows: the cooled gas exerts the preshock ram pressure on the galaxy interstellar gas and sweeps it up into a thick shell ('snowplow'), whose motion drives a milder outward shock into the ambient interstellar medium

- Cooling: IC (dominance) + Free-Free
  the radiation field of an Eddington accreting SMBH has $T \sim 10^7 K$. For shocks close to the SMBH, this radiation field is sufficiently intense that IC cools the electrons of the postshock wind gas more rapidly than the flow time.

$$T_{\text{shock}} \sim \frac{3}{16} \frac{\mu m_H}{k_B} v^2 \sim 1.6 \times 10^{10}\ \text{K},\ v \sim 0.1c$$

$$\mu: \ mean\ molecular\ weight\ of\ ionizing\ gas: \ 0.63$$

$$Radiative\ cooling\ time\ t_{rad} \sim 2 \times 10^{11} M_8^{-1} R_{kpc}^2 yr$$

$$Compton\ cooling\ time\ t_C = \frac{3 m_e c}{8\pi \sigma_T U_{rad}} \frac{m_e c^2}{E}$$

$$U_{rad} = \frac{L_{Edd}}{4\pi R^2 c b} b = \ covering\ factor$$

$$L_{Edd} = \frac{4\pi G c m_P M}{\sigma_T} \quad (77)$$

$$t_C = \frac{2}{3} \frac{cR^2}{GM} \left(\frac{m_e}{m_p}\right)^2 \left(\frac{c}{v}\right)^2 \quad b \sim 10^7 R_{kpc}^2 b M_8^{-1} yr \quad (78)$$

The cooling timescale t_s is :

$$\begin{aligned} t_{\rm flow} &= \frac{R}{\dot{R}} = 5\times10^6 R_{kpc}\sigma_{200}M_8^{-1/2} yr \\ t_s &= \frac{t_C}{t_{flow}} = 2R_{kpc}\sigma_{200}^{-1}M_8^{-1/2} b \propto R_{out} \end{aligned} \tag{79}$$

- From momentum-driven outflows to $M-\sigma$ relations:

$$M_\sigma = \frac{f_g k}{\pi G^2}\sigma^4 \sim 3.2\times10^8 M_\odot \sigma_{200}^4 \tag{80}$$

$$\begin{aligned} &\frac{d}{dt}(R\dot{R}) + \frac{GM}{R} = -2\sigma^2\left(1-\frac{M}{M_\sigma}\right) \\ &M < M_\sigma \rightarrow \ddot{R} < 0 \end{aligned} \tag{81}$$

$M < M_\sigma$:
1. the Eddington thrust (push) of the BH wind is too small to lift its weight against the galaxy bulge potential
2. the swept-up shell of interstellar gas cannot reach a large radius.
3. The SMBH cannot remove the gas from its surroundings and goes on accreting.
4. The swept-up shells fall back into fragments probably used for star formation.
$M > m_\sigma$:
1. the wind drives the swept-up ISM far from the nucleus, quenching its own gas supply and further accretion.

From momentum-driven to energy-driven: Momentum-driven conditions hold for the regions within 1 kpc of the AGN and establish the $M-\sigma$ relation. Once the SMBH mass attains the critical $M-\sigma$ value, the shocks move further from the AGN and the outflow becomes energy driven (e.g., large-scale molecular outflows that probably are able, at least at some level, to clear the galaxy from the gas).

- Energy output rate:
The coupling between the luminosity of the SMBH and the momentum-driven outflow is very inefficient. The impact on the host is limited.
This regime is a stable environment for BH mass growth $\Rightarrow$ we need outflows at a large scale to quench star-forming.

$$\begin{aligned} &M_{BH} \sim 3\times10^8 M_\odot \sigma_{200}^\alpha \\ &\dot{E_M} = \frac{1}{2}p_W v_M = \frac{L_{Edd}v_M}{2c} \\ &= \frac{1}{\sqrt{2}}\left(\frac{\sigma}{c}\right)L_{Edd}\left(\frac{M}{M_\sigma}\right)^{1/2} \\ &\sim 5\times10^{-4}\sigma_{200}L_{Edd}\left(\frac{M}{M_\sigma}\right)^{1/2} \propto M^{1/2} \end{aligned} \tag{82}$$

B. **energy-driven outflows**:

- Feature: transfer energy, thermal pressure is larger than ram pressure. Inefficient cooling. $\Rightarrow$ much more violent than momentum-driven flows.

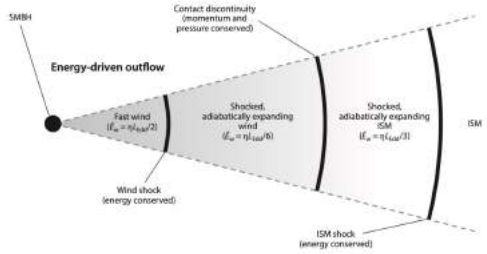

Figure 77: In an energy-driven outflow, the shocked regions are much wider and do not cool. They expand adiabatically, communicating most of the kinetic energy of the wind to the outflow. The outflow radial momentum flux is, therefore, larger than that of the wind

- Luminosity and Energy:

$$\begin{aligned} &\frac{d}{dt}\left[M_g(R)\dot{R}\right] + \frac{GM_g(R)M(R)}{R^2} = 4\pi R^2 P \\ &Neglect\ M = M_{BH}. \end{aligned} \tag{83}$$

Energy equation

$$\frac{d}{dt}(V\,U) = \frac{1}{2}\dot{M}_{out}v^2 - P\frac{dV}{dt} - \frac{GM_g(R)M(R)}{R^2}\dot{R}$$

Variation of internal energy | Rate of injection of energy into the shocked gas | Rate of work against the ambient gas | Rate of work against gravity

Figure 78: energy equation of energy-driven outflows

$$\begin{aligned} M_{\text{energy driven}} &= \frac{3f_g k\sigma^2\widehat{v}_e^3}{\pi G^2 c\eta} \sim \frac{3f_g k\sigma^5}{\pi G^2 c\eta} \\ &= \frac{3\sigma}{\eta c}M_\sigma \sim 6\times10^6 M_\odot\sigma_{200}^5 \end{aligned} \tag{84}$$

$v_e \sim \sigma$.

- Energy-driven outflows doesn't reproduce $M-\sigma$ relations:
$L_{mechanical}$ $\Rightarrow$ shock $\Rightarrow$ adiabatically expand into ISM :
Adiabatically expanding shocked gas pushes the ISM away as a hot atmosphere for any SMBH mass. Even if the AGN is switched off, the residual gas pressure still drives the outflow for a long time.

$$\begin{aligned} &L_{BH,Wind} \sim 0.05L_{edd} \propto 100E_{GAS} \\ &M_{energy-driven} \sim 6\times10^6 M_\odot\sigma_{200}^5 \\ &\dot{P}_{\rm out} = \dot{M}_{\rm out}\,v_{\rm out} \sim 20L_{Edd}/c >> \dot{P}_{mom} \sim \frac{L_{edd}}{c} \end{aligned} \tag{85}$$

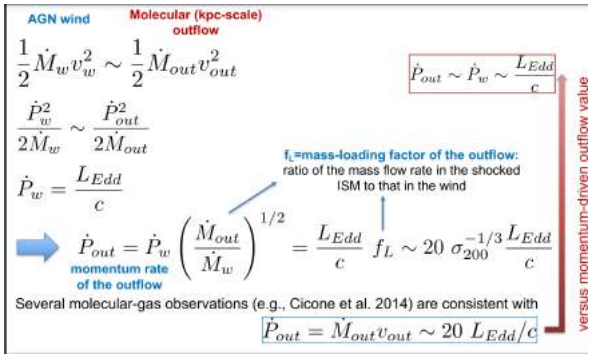

Figure 79: momentum rate of energy-driven outflows

- Outflows in [0III] may link with radio emission

10.2.2 Kinetic/Radio Mode:

- R_{edd} *low*
- parsec-scale jets produce over-pressured cavities.

10.3 Observation results in different scales

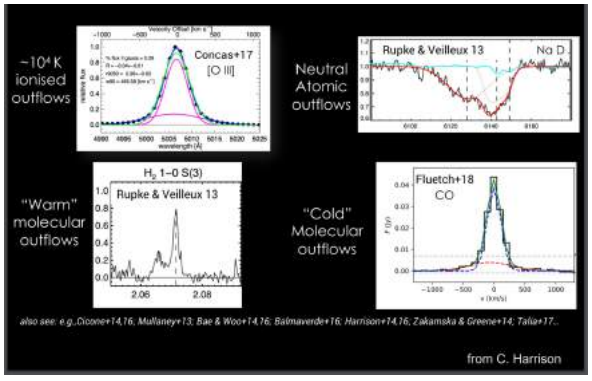

Figure 80: outflow observations in different bands

11 Supermassive Black Hole Mass

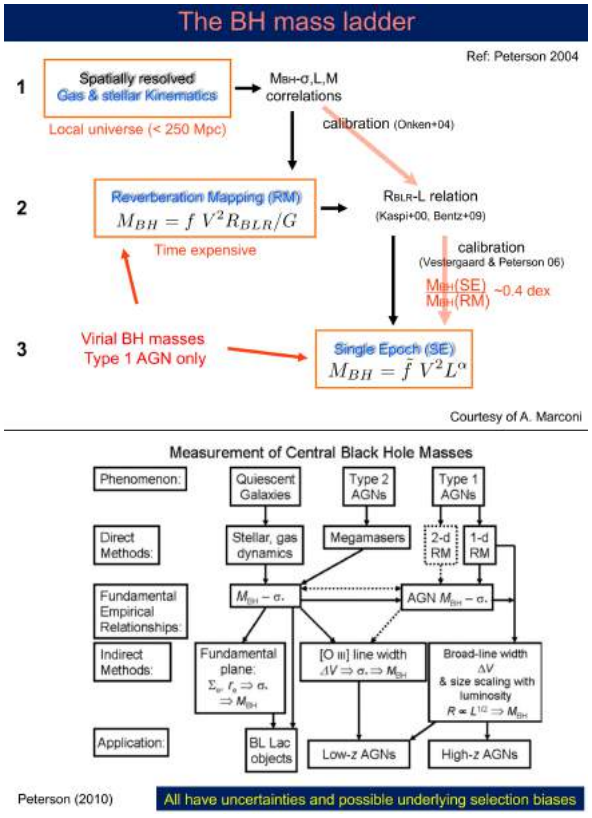

Figure 81: ladder of BH mass measurement

11.1 Direct methods: stellar dynamics, gas dynamics, RM

11.1.1 Sellar Dynamics: $R_{influence}$ of BH and angular resolution

The influence radius of the BH:

$$R_{BH} = \frac{GM_{BH}}{\sigma_\star^2} \sim 100 \left(\frac{M_{BH}}{10^9 M_\odot}\right)\left(\frac{200\ \mathrm{km/s}}{\sigma_\star}\right)^2 pc$$

Need high resolution, only for nearby objects :

$$\Delta\theta \sim 0.1'' \left(\frac{M_{BH}}{10^9 M_\odot}\right)\left(\frac{200\ \mathrm{km/s}}{\sigma_\star}\right)^2 \left(\frac{200Mpc}{D}\right) \quad (86)$$

Distance limit:

11.1.2 M-σ relation

- Applied to quiescent galaxies and weekly emitting AGN. Because luminous AGN will probably overwhelm the stellar light from BH influence shpere.
- observable: average velocity and velocity dispersion
- Tracer: stellar absorption features ⇒ stellar kinematics.
  emission line features ⇒ gas kinematics.

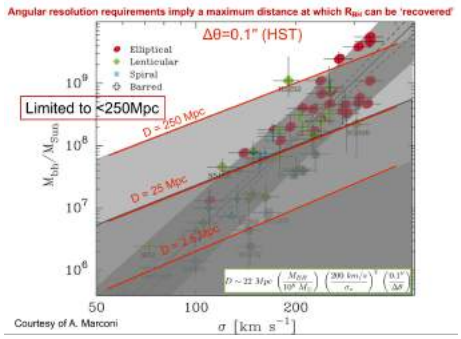

Figure 82: distance limit for Hubble

11.1.3 RM Technique

Time delay of the broad lines responds to continuum flux changes.

$$M_{BH} = f\frac{V^2 R}{G} \quad (87)$$

$R = R_{blr} = c\Delta\tau$.
f=3 for isotrope case.
For disc-shaped BLR case:

$$f = \left[\left(\frac{H}{R}\right)^2 + \sin^2(\theta)\right]^{-0.5} \quad (88)$$

From virial theorem: $V(FWHM)^2\tau = const.$ boarder lines, a shorter time. $\Delta\tau_{mean} \sim R/c$
More reliable method: σ from RMS spectrum: Using

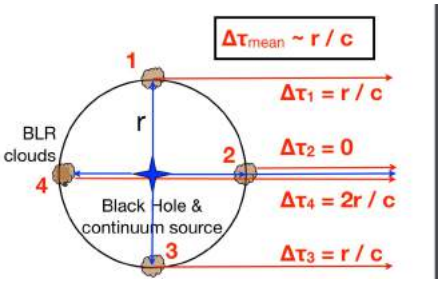

Figure 83: RM time

the average spectrum of N observations.

$$\overline{F(\lambda)} = \frac{1}{N}\sum_{i=1}^{N} F_i(\lambda)$$
$$S(\lambda) = \left(\frac{1}{N-1}\sum_{i=1}^{N}\left[F_i(\lambda) - \overline{F(\lambda)}\right]^2\right)^{1/2} \quad (89)$$

For RMS spectrum, only the parts of the emission lines which are varying are measured.
In reality, we integrate all is delay surfaces to get the emission-line light curves.

$$L(t) = \int_{-\infty}^{\infty} \Psi(\tau)C(t-\tau)d\tau \quad (90)$$

1. BLR:

- Feature: $n_H \sim 10^{11} cm^{-3}$, $T \sim 10^4 K$, characteristic distance: $r \sim 10^{17} cm \sim 10^{-1} pc$, $\sim 700 R_g$ for 10^9 $M_\odot$ BH.

- BLR is in photoionization equilibrium:

$$U = \frac{Q_{ion}}{4\pi R^2 n_e c} \quad \text{Ionization parameter}$$
$$Q_{ion} = \int_{h\nu > E_{ion}} \frac{L(\nu)}{h\nu} d\nu \quad \text{Number of ionizing photons} \tag{91}$$

- Velocity of BLR: BLR is inside the BH influence sphere ($r_{BLR} << r_{BH}$)

$$V_K \sim 1.6 \times 10^4 \left(\frac{M_{BH}}{10^9 M_\odot} \frac{20ld}{R} \right)^{1/2} \text{ km/s} \tag{92}$$

- Assume all AGN spectra have similar U, n_e and $Q_{ion}/\lambda L_\lambda$ ratio. Then we can get scaling relation of $R - L$.

$$L/R^2 \sim \text{ cons } \rightarrow R \propto L^{0.5} \tag{93}$$

11.2 Indirect Methods: Broad line widths, scaling relation

11.2.1 Scaling Relation

$R \propto L^\alpha$

11.2.2 Single-epoch Virial Method

- Scaling relations requiring FWHM and L_{cont}.

- Assumption: BLR clouds in Keplerian orbital motion: Dynamics is dominated by the BH gravitational field.

- Typical lines:$H\beta 4863$, $MgII 2798$, $CIV 1549$**(blueshifted due to outflows),** $5100, 3000, 1350$ **for continuum**.

$$\log\left(\frac{M_{BH}}{M_\odot}\right) = A + 2\log\left(\frac{FWHM}{1000 km/s}\right) + B\log\left(\frac{\lambda L_\lambda}{10^{44}\text{erg/s}}\right) \tag{94}$$

- For obscured AGN: Near-IR Paschen lines. Hard X-ray luminosity instead of opt./UV luminosity.

$$\log\left(\frac{M_{BH}}{M_\odot}\right) = 7.75 + \log\left[\left(\frac{FWHM_{NIR}}{10^4 \text{ km/s}}\right)^2 \left(\frac{L_{14-195keV}}{10^{42}\text{erg/s}\,|}\right)^{0.5}\right] \tag{95}$$

- Weakness:

- The radiation pressure experienced by the electrons in the BLR may play a role in determining the kinematic properties of the BLR clouds (Marconi et al. 2008; Chiaberge & Marconi 2011), which would provide an under-estimation of the BH mass derived using SEV.
  $M_{BH}=f\Delta v^2$ R/G + gL, where **gL** is the term of P_{rad}; g∝1/4πGcm$_p$N$_H$ → probably MgII line, being characterized by larger N$_H$ than Hβ and CIV, is less affected by radiation-pressure effects – Marconi+12)
- Broad lines can show asymmetries which may affect the black hole mass estimate. Broad/narrow line decomposition is not unique, and a line profile should be assumed
- Host-galaxy starlight may contaminate the continuum emission. Similarly, jet emission in radio-jetted AGN may provide a further source of contamination

Figure 84: issues of SEV methods

12 Tips for Sgr A and M87

12.1 Properties of Sgr A

1. General Properties of Sgr A^*:
   - Mass $4.3 \times 10^6 M_\odot$
   - D: 8kpc
   - L_{X-ray}: 10^{33}erg/s
   - Daily X-ray flares $\leq 10^{35} ergs^{-1}$
   - $L_{edd} \sim 10^{44}$erg/s
2. X-ray emission: diffuse emission
   - Soft emission ($kT \simeq 0.8 - 1keV$): SN activity
   - $kT \simeq 7 - 8keV$ plasma with ionized Fe emission at 6.7keV: faint X-ray sources.
   - Fe fluorescence lines are bombarded by X-rays from a transient source (Sgr A)
   - Clumpy 6.4keV component: molecular clouds and reflection

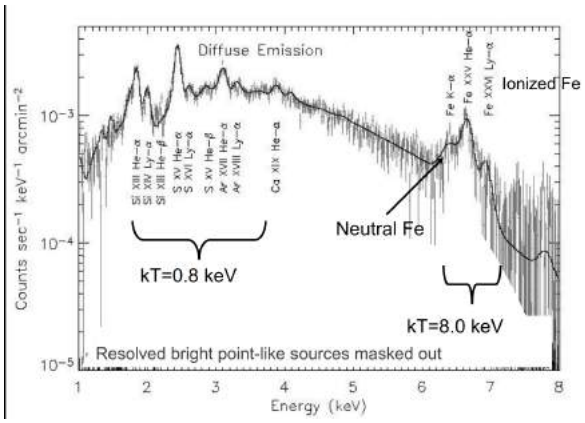

Figure 85: GC diffuse x-ray emission

- The diffuse X-rays trace the distribution of stars, not the ISM. Diffuse X-rays associated with the old population of the Galactic bulge. Some of the diffuse features also trace the sites of recent star formation.

12.2 Molecular Clouds

- Iron fluorescence from molecular clouds:
  Produced when neutral iron in molecular clouds with $N_H \sim 10^{23} cm^{-2}$ is bombarded either by photons or electrons.
- XRN Model(x-ray reflection nebula): molecular clouds as mirrors of past activity:

$$L_{\mathrm{SgrA}^*} \propto \frac{d^2 \times I_{FeK}}{r^2 \times n_H} \tag{96}$$

reflected emission from the past outburst of an x-ray source

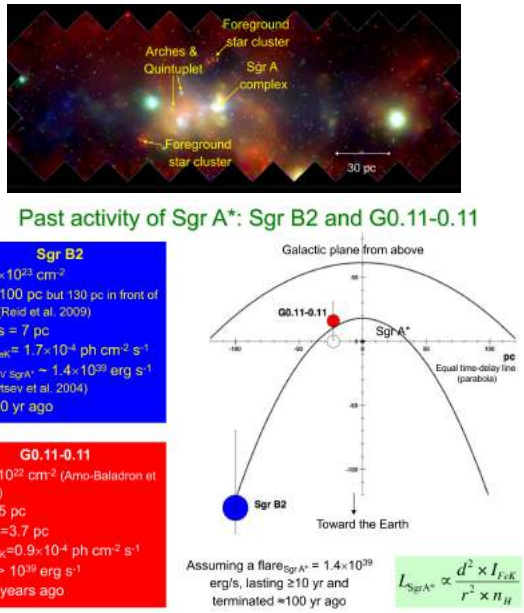

Figure 86: light echoes for a post-burst activity

- Alternative model of XRN: cosmic rays
  Neutral Fe line consistent with being produced by low-energy hadronic cosmic rays LECRs (i.e., bombardment of molecular clouds by energetic ions), accelerated in the bow shock resulting from the cluster's proper motion against the MC.

12.3 Transcient X-ray Flares

1. period: at least 1/day (rare in this high time frequency)
2. Power: brighest flare reaches $\sim 10^{36} erg/s$
3. Each X-ray flare has an IR flare The opposite not necessarily true Complex variability pattern
4. possible mechanism: IR $\rightarrow$ X-ray
   - population of electrons undergoing continuous acceleration due to turbulent processes in the inner accretion flow. IR connected to X-rays through models of pure synchrotron, SSC, and IC (all viable).

12.4 Transient X-ray outbursts

- Duration: a few years.
- Transient X-ray emission: Magnetars are expected (e.g. possible: SGR J1745-2900.III).See87

12.5 Fermi Bubbles and X-ray Extension

1. Likely mechanism of Fermi Bubble:
   - IC emission from CR electrons on the CMB photons + photons from other radiation fields.
   - Unkown but close to Sgr A.
   - Radio bubbles can be combined with weaker and steadier outflows.

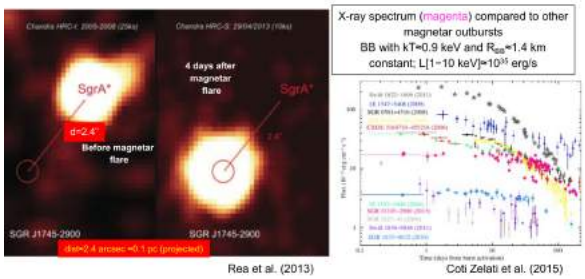

Figure 87: Megnetar outburst vs XRB

2. Properties of Fermi Bubble:
   - scale: $\sim 10kpc$ above and below
   - L $\sim 10^{37}$erg/s in total
   - Shape: sharp edges + flat profiles. Flat spectrum
3. X-ray chimneys:
   - Likely mechanism: powerful outflows associated with a series of past episodic events connecting the GC with the halo

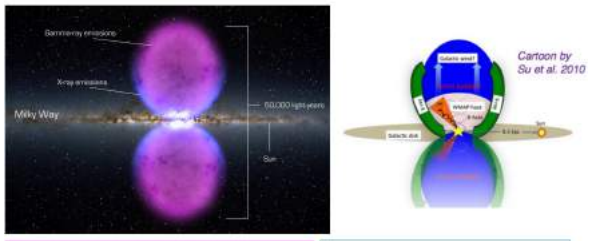

Figure 88: Fermi Bubble

12.6 EHT Observation of M87

1. 3 Requirements of EHT observation:
   - Sufficient number of emitted photons
   - Emission coming close enough to the BH to be gravitationally lensed around it
   - The surrounding plasma is sufficiently transparent at the observed frequency
   - High resolution.
   - M87 is Low-L AGN and in ADAF accretion: millimeter observations are needed
2. Why M87?
   with the largest apparent angular sizes.
3. Photon Capture radius:
   $R_c = \sqrt{27}R_G$ (For non-rotating Schwarschild BH)
   - $r < R_c$: captured into BH
   - $r = R_c$: captured on an unstable circular orbit and produce a lensed photon ring
   - For accreting BHs embedded in a geometrically thick, optically thin emission region (LLAGN case), the combination of an event horizon and light bending leads to the appearance of a dark shadow along with a bright emission ring

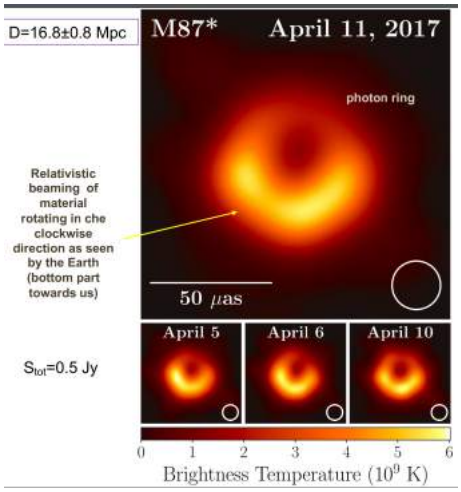

Figure 89: EHT Observation result

References